Am J Cancer Res 2022;12(8):3892-3912
www.ajcr.us /ISSN:2156-6976/ajcr0144138

Original Article

Prrx1 promotes resistance to temozolomide by upregulating ABCC1 and inducing vasculogenic mimicry in glioma

Zetao Chen[1*], Yujie Zhang[2,3*], Yihong Chen[1*], Wanmei Lin[2,3], Yuxuan Zhang[1], Guixing Cai[2,3], Xinlin Sun[1], Kehong Zheng[4], Jie He[2,3], Tianjing Ai[2,3], Jihui Wang[1], Liang Zhao[2,3], Yiquan Ke[1]

[1]The National Key Clinical Specialty, Department of Neurosurgery, Zhujiang Hospital, Southern Medical University, Guangzhou, China; [2]Department of Pathology, Nanfang Hospital, Southern Medical University, Guangzhou, China; [3]Department of Pathology, School of Basic Medical Sciences, Southern Medical University, Guangzhou, China; [4]Department of General Surgery, Zhujiang Hospital, Southern Medical University, Guangzhou, China. [*]Equal contributors.

Received May 14, 2022; Accepted July 25, 2022; Epub August 15, 2022; Published August 30, 2022

Abstract: Gliomas are the most common primary brain tumors with dismal prognoses. Temozolomide (TMZ), the frontline therapeutic agent for gliomas, has shown limited clinical benefit primarily due to the acquired chemoresistance. Although growing evidence has suggested that the multi-drug resistance phenotype and abnormal vascular microenvironment are responsible for the intrinsic and extrinsic TMZ resistance, the molecular mechanism of TMZ resistance remains to be elucidated. In this study, we found Paired-related homeobox 1 (Prrx1) was an independent prognostic factor for the efficacy of chemotherapy-based postoperative treatment. Silencing Prrx1 markedly enhanced the TMZ-induced cytotoxicity both in vitro and in vivo. We also demonstrated that Prrx1 increased the expression of ABCC1, a member of ATP-Binding Cassette (ABC) transporter protein family, through binding to the promoter region of ABCC1 gene and initiating its transcription. Silencing ABCC1 mitigated the TMZ resistance induced by Prrx1. Furthermore, Prrx1 facilitates the formation of vasculogenic mimicry (VM), a critical extrinsic mechanism for glioma TMZ resistance. Collectively, our findings supported the critical role of Prrx1 in TMZ resistance via intrinsic and extrinsic mechanism. Targeting Prrx1 might represent a feasible strategy to overcome therapeutic resistance in glioma.

Keywords: Prrx1, MDR, ABCC1, vasculogenic mimicry, TMZ resistance

Introduction

Gliomas are the most prevalent primary intracranial tumors, accounting for 70-80% of all brain tumors. Among them, glioblastoma (GBM) is the most malignant subtype with an overall median survival time of less than 15 months and a 5-year survival rate of less than 10% [1]. Despite a variety of standard of care, such as surgery, temozolomide (TMZ, a frontline treatment for gliomas) chemotherapy, radiation, and various targeted therapies including antiangiogenic therapy, have been applied to GBM treatment, therapeutic resistance inevitably develops, and the prognosis remains dismal [2]. And the molecular mechanisms of therapeutic resistance in GBM remain poorly understood.

As an alkylating agent, TMZ requires the formation of O6-meG to be effective and to induce apoptosis. Meanwhile, MGMT is the enzyme that repairs the cytotoxic O6-meG generated by TMZ. Methylation on the promoter of MGMT is associated with the enhanced sensitivity of glioma cells to TMZ and a prolonged survival time of patients with gliomas [3]. In addition to TMZ, gliomas also display resistance to a broad spectrum of drugs that are structurally and morphologically different. This property is known as Multiple Drug Resistance (MDR) that involves the activation of diverse resistance mechanisms [4]. The acquisition of the MDR phenotype in glioma has been highly related to the overexpression of ATP-Binding Cassette (ABC) transporters, which can extrude antitu-

mor agents, decrease their intracellular concentration, and consequently attenuate their therapeutic efficacy [5]. In human genome, the ABC transporter superfamily is composed of 48 members that are classified into seven subfamilies, from ABC-A to -G, based on their sequence homology [6]. Many studies have demonstrated the role of ABCC1, a crucial member of the ABC transporter protein family, in the MDR of several types of solid tumors, including non-small-cell lung cancer [7], colon cancer [8] and breast cancer [9]. In supporting this notion, in some instances, downregulation or inhibition of ABCC1 could provide therapeutic benefit [10]. Notably, both retrospective and prospective studies have shown that the high expression level of ABCC1 is a reliable independent prognostic indicator of poor outcome in primary neuroblastoma [11, 12].

Apart from the abovementioned intrinsic chemoresistance mechanism, extrinsic factors also contribute to the resistance of glioma cells to TMZ. Malignant gliomas rely on angiogenesis to establish a source of nutrients and oxygen as well as to eliminate cellular waste products [13]; simultaneously, these excessive aberrant vessels obstruct the transportation and distribution of chemotherapeutics and ultimately lead to chemoresistance [14]. However, conventional anti-angiogenic therapies such as bevacizumab, which only focus on the classical endothelium-dependent vessels (EDVs), fail to achieve survival benefits in gliomas [15, 16], suggesting a novel mechanism of escape underlying perfusion of the tumors that bypasses the classical ECs-mediated EDVs. Indeed, a novel microcirculation model named vasculogenic mimicry (VM) has been found to be responsible for the failure of conventional anti-angiogenic therapy. Distinct from the classical EDV, VM refers to a tumor microcirculation pattern in which highly plastic tumor cells aggregate, migrate and remodel to form vascular-like structures which facilitate the supply of nutrients and oxygen. Although cumulative studies have established that both upregulation of ABC transporter proteins and VM formation lead to TMZ resistance, the underlying molecular mechanism still needs to be further elucidated.

Paired-related homeobox 1 (Prrx1) is a homeodomain transcription factor originated from the mesoderm and is widely recognized as an EMT (Epithelial-Mesenchymal Transition) and stemness inducer in a variety of solid tumors. Previous studies on gliomas also reveal that Prrx1 promotes the tumorigenicity of glioma stem cells (GSCs) [17] and the invasive properties of GBM cells in vitro [18]. Based on the above studies, we have recently reported the involvement of Prrx1 in glioma stemness and angiogenesis via activating TGF-β/Smad pathway and upregulating proangiogenic factors. Interestingly, it has previously been observed that GSCs present elevated expression of ABC transporter proteins. Additionally, several lines of evidence have supported the notion that, under therapeutic stress, GSCs are transdifferentiated into endothelial-like cells, which is a major mechanism of VM formation [19]. Therefore, we hypothesized that Prrx1 might promote TMZ resistance through upregulating ABC transporter proteins and regulating the GSCs-based VM formation.

Herein, we demonstrated the critical roles of Prrx1 in therapeutic resistance of gliomas. Our current study revealed that Prrx1 not only upregulated ABCC1 through binding to its promoter, but also promoted VM formation by supporting the plasticity of glioma cells and remodeling extracellular matrix. The enhanced expression of ABCC1 and formation of VM synergistically contributed to TMZ resistance in gliomas via intrinsic and extrinsic mechanisms. Hence, our study has elucidated a novel mechanism of TMZ resistance in gliomas, providing the rationale for targeting Prrx1 as a feasible strategy to overcome TMZ resistance.

Materials and methods

Cell culture and human tissue samples

Human glioma cell lines U251, U87MG, LN229 and human embryonic kidney 293T cells were purchased from the American Type Culture Collection (ATCC). The U87-Luc cell line was generated in our laboratory via transfection with a reporter gene encoding firefly luciferase as previous described [ref]. All cells were cultured in Dulbecco's modified Eagle's medium (DMEM, Thermo Scientific, Waltham, MA, USA) supplemented with 10% fetal bovine serum (FBS, Thermo Scientific, Waltham, MA, USA), 100 IU/mL penicillin G, and 100 μg/mL streptomycin (Invitrogen Life Technologies, Carlsbad, CA, USA). Cells were maintained in a humidified

atmosphere containing 5% CO_2 at 37°C. All cell lines used in this study were authenticated within four years by short tandem repeat (STR) profiling, and experiments were performed in cells < 6 months in culture. A total of 72 formalin-fixed, paraffin-embedded glioma samples were obtained from patients undergone surgical treatment at Zhujiang Hospital, Southern Medical University. Both study protocol and informed consent were approved by the Ethical Committee of Zhujiang Hospital. The expression profiling of target genes on glioma samples were identified through database search in GEO: GSE4412 (n = 85), GSE42669 (n = 58), GSE13041 (n = 267) and GSE4290 (n = 180).

Lentiviral infection and siRNA transfection

The lentivirus plasmids expressing Prrx1 or Prrx1 short hairpin RNA (shRNA) were constructed as reported previously [20]. Cells were infected with lentivirus and polybrene for 24 h. Cells stably expressing vector, Prrx1, or shPxrx1 were selected and maintained in puromycin-containing medium (2 μg/mL, Solarbio, China). The siRNA of ABCC1 and scramble sequences as negative control were purchased from Hanbio (Shanghai, China) and transfected using the lipofectamine® 3000 reagent (Cat# L3000015, Thermo Fisher Scientific, USA).

TMZ chemosensitivity and cell viability assay

Cells were seeded in 96-well plates and treated with TMZ at different concentrations (0, 100, 200, 300, 400, and 500 μg/ml) for 48 h, followed by incubating with fresh medium containing 10% CCK-8 solution for 2 h (Dojindo, Kumamoto, Japan). The absorbance was measured at 450 nm by using Ultra Multifunctional Microplate Reader (Tecan, Switzerland), and the IC50 values were calculated to evaluate the cell sensitivity to TMZ.

Flow cytometry for cell apoptosis

Cells were seeded in six-well plates, treated with TMZ (200 μg/ml) for 48 h, and harvested for further analysis. Cell apoptosis was detected using APC/PI Apoptosis Detection Kit (BD Pharmingen, USA) according to the manufacturer's instructions. Apoptotic cells were analyzed by FACS cytometry (BD Biosciences Inc., Franklin, NJ, USA).

Colony formation assay

About 1500 cells were seeded in 35 mm culture dishes and treated as indicated in the figures. The cells were cultured continuously until visible colonies formed. The cell culture dishes were then fixed with methanol and stained with 0.1% crystal violet for the visualization of colonies. The number of colonies was counted and analyzed statistically.

Tube formation assay

Growth factor reduced Matrigel (BD Biosciences, USA) was prepared and kept on ice until use. Matrigel solution (50 μl) was added evenly to the well of 96-well plate and incubated at 37°C for 150 min. Tumor cells (2×10^4) were incubated in 200 μl endothelial cell growth medium-2 (EGM-2) for 12 h before image taking. The capillary tubes were quantified by measuring the total numbers of the completed tubule structure under a 100× bright-field microscope. Each experiment was repeated three times.

Cell migration and invasion assay

Migration assay was performed using Transwell chambers in 24-well plates (pore size of 8 μm, Costar, USA). Complete medium with 10% FBS was added to the bottom wells of the chambers as a chemoattractant. Cells (1×10^5) were resuspended in 100 μl serum-free medium and added to the upper chamber. The invasion assay was similarly performed except the chamber insert was coated with Matrigel. After incubation at 37°C for 24 or 48 h, the migrated or invaded cells on the lower membrane were fixed with methanol, stained with crystal violet, and counted under a light microscope in five random visual fields (× 200).

RNA isolation, reverse transcription, and quantitative real-time PCR

Total RNA was extracted using Trizol (Invitrogen, Carlsbad, California). To quantify the expression of indicated genes, the total RNA was reverse transcribed (RT) using a ThermoScriptTM RT-PCR System (Invitrogen). Real-time polymerase chain reaction (PCR) was carried out using an SYBR Green PCR master mix (Applied Biosystems, Foster City, California) on an ABI 7500HT system. GAPDH was used as an

endogenous control. All samples were normalized to internal controls for normalization, and fold changes were calculated through relative quantification ($2^{-\Delta\Delta CT}$). The primers used were shown in Supplementary Table 4.

Western blot

RIPA lysis buffer with protease inhibitor cocktail was used to extract total proteins. Proteins were quantified by BCA protein assay kit (Pierce, KeyGEN BioTECH, Jiangsu, China) before separated by SDS-PAGE gel and transferred onto the PVDF membrane (Millipore, Darmstadt, Germany). The membrane was blocked with 5% nonfat milk in TBST at 4°C overnight, followed by incubation with primary antibodies against Prrx1 (ABclonal, 1:1000), CD144, MMP2, MMP9, GAPDH and β-tubulin (1:1000, Proteintech) at 4°C overnight. After extensive washing, the membranes were incubated with the appropriate HRP-conjugated secondary antibodies for 1 h at room temperature. The signal was detected by the enhanced chemiluminescence detection system (Tennon5200, Shanghai, China).

Immunohistochemical staining

Specimens of surgically dissected tumors from glioma patients and glioma xenograft mice were fixed with 4% formalin, paraffin embedded, and sectioned (4 μm). The tissue sections were then deparaffinized and dehydrated followed by incubation in 3% hydrogen peroxide for 10 min. Slides were stained with primary antibodies against Prrx1 (Abcam, 1:200), CD31 (1:100, ZSGB Bio), SOX2 (1:300, Proteintech), Ki67 (1:100, ZSGB Bio), ABCC1 (1:300, Proteintech) at 4°C overnight after blocking with 5% BSA in PBS at RT for 1 h (Room Temperature). Appropriate secondary antibodies were used at RT for 1 h. The signals were detected by DAB staining using an IHC detection kit. CD31-PAS dual staining for VM detection was performed as previously described [49]. Slides were counterstained with hematoxylin. Two investigators without prior knowledge of samples independently either performed the staining or analyzed the glioma tissue section.

Animals and intracranial xenograft

Four- to six-weeks-old Balb/c male nude mice were purchased from the Central Animal Facility of Southern Medical University. The protocols for animal study have been approved by the Animal Care and Use Committee of Southern Medical University. U87-Luc cells stably expressing shPrrx1 or control vector were injected stereotactically into the right hemicerebrum of Balb/c nude mice. Each group included 6 mice. Tumor growth was monitored using an in vivo imaging system (IVIS Lumina II, Caliper, USA) after an intraperitoneal injection of luciferase substrate-D-luciferin (YEASEN, Shanghai, China). For drug inhibition assay, mice were randomized into indicated group (6 mice per group) 7 days after intracranial implantation. All groups of mice were administered three times a week for 3 weeks with: (a) DMSO; (b) TMZ (10 mg/kg, i.p.). Mice with neurological deficits or moribund appearance were sacrificed. The tumor-bearing brains were sectioned for immunohistochemical or immunofluorescence analysis.

Luciferase reporter assays

ABCC1 was predicted to be the target gene of Prrx1 by using JASPAR software (http://jaspar.genereg.net/). A 2000-bp fragment containing two potential Prrx1-binding sites from the ABCC1 promoter (named WT) was PCR-amplified and cloned into a pGL3 luciferase reporter vector. In addition, a mutant with Prrx1-binding site mutations (Mutation-1: Δ (256-263), Mutation-2: Δ (774-781)) was generated from the WT construct. Each pGL3 plasmid was co-transfected with Prrx1-overexpression vector into 293T and LN229 cells using the lipofectamine® 3000 reagent (Thermo Fisher Scientific, USA). Luciferase activity was measured at 48 h after transfection using the Dual-Luciferase Reporter Assay System (Promega Corporation, Madison, WI, USA).

Chromatin immunoprecipitation (ChIP) assay

Standard CHIP assay was performed following the manufacturer's instructions (Pierce Agarose ChIP Kit, Thermo Scientific, Waltham, MA, USA). Briefly, after cells were cross-linked and lysed, genomic DNA was sonicated on ice to produce DNA fragments about 200 to 1000 bp long. Anti-HA antibody (1:50, Abmart) and control immunoglobulin G were used to precipitate protein-DNA complexes. Finally, PCR was carried out to examine the putative Prrx1-binding sites

on the ABCC1 promoter with specific primers (Supplementary Table 5).

Statistical analysis

The data were analyzed using SPSS version 19.0 software (SPSS, Chicago, IL, USA). Sample size for each study was determined based on the information reported, and no statistical method was used to predetermine sample size. The clinical data were analyzed using nonparametric tests and Kaplan-Meier survival analysis. Pearson's chi-squared (χ^2) test and student's t-test were used to evaluate the significance of the differences among different groups. All statistical tests were two-sided. The data were presented as the means ± SD.

Results

Prrx1 functioned as an independent predictor for the efficacy of chemotherapy-based postoperative treatment in glioma patients

To identify candidate genes associated with chemotherapy efficacy in glioma, we first conducted differentially expressed gene (DEG) analysis in dataset GSE4290 containing 23 noncancerous and 157 glioma samples. The top 50 upregulated and downregulated DEGs were chosen for univariate cox regression analysis in chemotherapy-based postoperative treatment samples of CGGA cohort and REMBRANDT cohort. Genes with $P < 0.05$ were selected, and a total of overlapping 11 genes were identified including Prrx1 (**Figure 1A**). We subsequently performed univariate and multivariate Cox analysis to determine whether Prrx1 functioned as an independent predictor in glioma. Univariate Cox analysis demonstrated that high expression of Prrx1 was strongly correlated with poor overall survival (hazard ratio [HR] = 1.343, 95% CI = 1.112-1.620, p = 0.002). Multivariate Cox analysis confirmed Prrx1 as an independent predictor of prognosis for OS in glioma (HR = 1.821, 95% CI = 1.114-2.976, p = 0.017), as shown in **Tables 1** and **2**. According to the clinical data from CGGA database, we found that patients with high Prrx1 expression displayed a worse response to standard of care such as chemotherapy and radiotherapy (**Figure 1B**). Specifically, only patients with low Prrx1 expression could benefit from chemotherapy and could show significant survival improvement (**Figure 1C**). In addition, in GSE7696 and CGGA cohorts, Prrx1 expression levels were markedly higher in recurrent glioma specimens than in primary gliomas (**Figure 1D** and **1E**), suggesting the significant role of Prrx1 in response to therapeutic treatment in glioma. Furthermore, the gene set enrichment analysis (GSEA) was performed to investigate the potential regulatory role of Prrx1 in glioma. The results showed that multi-drug resistance pathway was positively enriched in patients with high Prrx1 expression (**Figure 1F**). Taken together, these findings suggested that Prrx1 might be involved in glioma therapeutic resistance.

Knockdown of Prrx1 markedly enhanced the sensitivity to TMZ in intracranial xenograft model

Based on the above bioinformatic analyses and clinical data, we next investigated whether downregulating Prrx1 affected TMZ efficacy *in vivo* by utilizing intracranial mouse models (**Figure 2A**). Bioluminescence analysis demonstrated that silencing of Prrx1 expression by shRNA markedly increased the efficacy of TMZ treatment in U87MG glioma cells-derived tumors as reflected by the change in tumor volume (**Figure 2B** and **2C**). Prrx1 silencing also markedly prolonged the survival time of intracranial xenograft mice receiving TMZ treatment compared to mice bearing U87MG-shNC tumors (**Figure 2D**, NC indicates Negative Control). These findings demonstrated that Prrx1 was involved in the development of TMZ resistance in glioma cells.

Prrx1 increases the resistance of glioma cells to TMZ in vitro

After having determined the importance of Prrx1 in the sensitivity of glioma cells to TMZ treatment in intracranial xenograft model, we confirmed this function of Prrx1 - *in vitro* in glioma cells. First, we constructed the Prrx1-overexpressing lentivirus (Prrx1-OE) and two independent Prrx1 shRNA-expressing lentivirus (shPrrx1-1 and shPrrx1-2). Glioma cell lines LN229 and U251 were used to overexpress or silence Prrx1, respectively, as previously described [20]. Transfection efficiency was confirmed by RT-qPCR (**Figure 3A**) and western blot (**Figure 3B**). The effect of Prrx1 on TMZ-induced cytotoxicity was quantified through generating dose-response curves. The calculated IC50

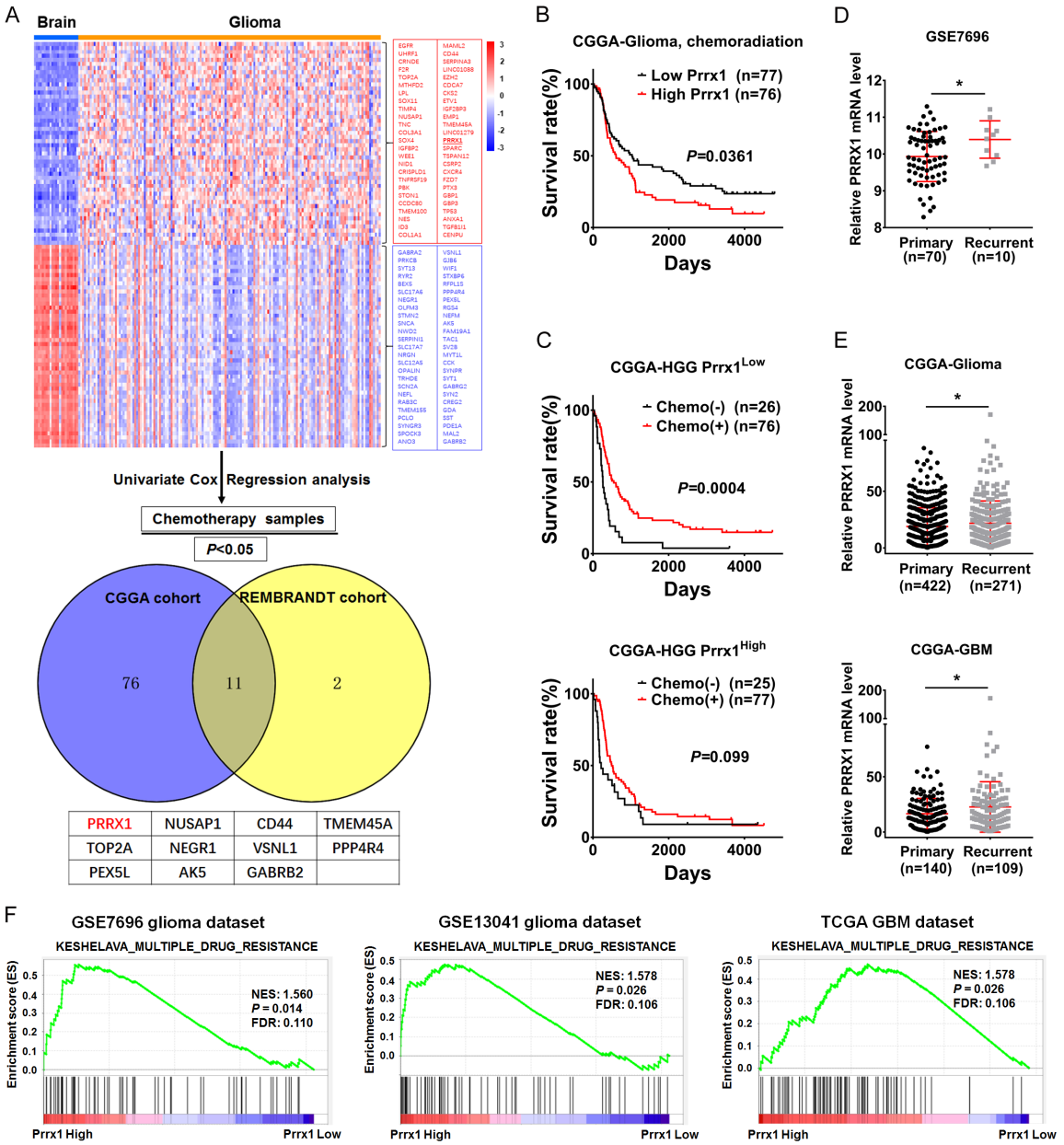

Figure 1. Elevated expression of Prrx1 predicted worse chemotherapy efficacy and multiple drug resistance in gliomas. A. Identification of candidate TMZ efficacy related genes in the GSE4290, CGGA and REMBRANDT datasets. B. Survival curves for chemoradiation-treated glioma patients with distinct Prrx1 expression level from the CGGA database. C. Glioma patients from the CGGA database were divided into $Prrx1^{Low}$ (above panel) and $Prrx1^{High}$ (below panel) groups based on the median expression level of Prrx1. The survival curves comparison between the chemotherapy-treated and nonchemotherapy-treated patients in each group. D. Scatter diagram represented Prrx1 expression level in human primary and recurrent glioma tissues from GSE7696 database. E. Scatter diagram represented Prrx1 expression level of human primary and recurrent glioma (above panel) and GBM (below panel) tissues from CGGA database. F. Gene set enrichment analysis (GSEA) demonstrated multiple drug resistance (MDR) pathways in high Prrx1 expression glioma group of multiple glioma datasets. *$P < 0.05$.

value of TMZ for LN229 cells was 238.7 μM; however, this value was elevated to 510 μM when Prrx1 was overexpressed in LN229 cells (**Figure 3C**, left panel). Conversely, IC50 was decreased in Prrx1-silenced U251 cells compared to vector-transfected cells (**Figure 3C**, right panel). Next, flow cytometry was performed to evaluate the apoptosis of Prrx1-overexpressed or Prrx1-silenced cells compared to their corresponding control cells. As shown in **Figure 3D**, the TMZ-induced apoptosis was negatively correlated with Prrx1 expres-

Table 1. Univariate and multivariate cox proportional hazards analysis of clinicopathological variables based on overall survival (OS) in the REMBRANDT TMZ chemoradio treatment glioma cohort (n = 102)

For OS variables	Univariate analysis			Multivariate analysis		
	HR	95% CI	*P* value	HR	95% CI	*P* value
Age	1.042	1.024-1.061	< 0.001	1.031	0.999-1.063	0.060
Gender	0.770	0.491-1.208	0.255	/	/	/
WHO Grade	2.080	1.362-1.362	< 0.001	1.118	0.592-2.109	0.731
KPS	0.191	0.056-0.648	0.008	0.307	0.057-1.658	0.170
PRRX1	1.343	1.112-1.620	0.002	1.823	1.116-2.979	0.017

Table 2. Univariate and multivariate cox proportional hazards analysis of clinicopathological variables based on overall survival (OS) in the CGGA TMZ chemoradio treatment glioma cohort (n = 153)

For OS variables	Univariate analysis			Multivariate analysis		
	HR	95% CI	*P* value	HR	95% CI	*P* value
Age	1.019	1.003-1.036	0.022	1.011	0.994-1.030	0.211
Gender	1.053	0.720-1.539	0.791	/	/	/
WHO Grade	2.617	1.957-3.500	< 0.001	1.775	1.294-2.437	< 0.001
PRS type	1.833	1.390-2.416	< 0.001	2.103	1.511-2.925	< 0.001
IDH mutation status	0.407	0.274-0.606	< 0.001	1.021	0.614-1.698	0.936
1p19q codeletion status	0.161	0.082-0.314	< 0.001	0.134	0.063-0.283	< 0.001
MGMTp methylation status	0.782	0.538-1.136	0.196	/	/	/
PRRX1	1.008	1.000-1.016	0.033	1.011	1.003-1.019	0.008

Abbreviations: OS, overall survival; HR, hazard ratio; CI, confidence interval; KPS, Karnofsky performance score; PRS, TMZ, temozolomide; For continuous variables, they are centered and scaled (standard deviation set to one) in the models, and HR is the relative hazard when increasing thevariable one standard deviation. All statistical tests were two sided.

sion level in glioma cells. Additionally, colony formation assay showed that the overexpression of Prrx1 in LN229 cells significantly increased the colony number both in TMZ-treated group and DMSO-treated control group compared to vector-transfected cells (**Figure 3E**, left panel). Opposite results were observed when Prrx1 was silenced in U251 cells (**Figure 3E**, right panel). These results indicated that Prrx1 was positively associated with the increased TMZ resistance of glioma cells *in vitro*.

Prrx1 directly bound to the promoter and up-regulated the expression of ABCC1

To elucidate the molecular mechanisms by which Prrx1 regulates TMZ resistance in glioma, we examined the correlation in expression level between Prrx1 and drug resistance genes, including ABCB1, GSTP1, BIRC5, ABCC1 and TOP2A by RT-qPCR. Increased expression levels of the above genes except TOP2A were observed in Prrx1-overexpressing LN229 cells (**Figure 4A**, left panel). This effect was attenuated when Prrx1 was silenced in U251 cells (**Figure 4A**, right panel). Among the drug resistance genes examined, the expression level of ABCC1 was one most significantly affected by Prrx1. Further analysis showed that ABCC1 upregulation was associated with worse prognosis in glioma receiving chemotherapy (**Figure 4B**). Additionally, the expression level of ABCC1 was significantly higher in GBM compared to normal brain tissue (**Figure 4C**). Kaplan-Meier survival analysis showed that higher expression of ABCC1 predicted poor overall survival (OS) and disease-free survival (DFS) (**Figure 4D**). Since Prrx1 was identified as both a homeodomain transcription factor and a chaperone protein involved in transcription factor activity, we speculated that Prrx1 might transactivate the expression of ABCC1. To test whether Prrx1 enhanced ABCC1 expression by directly binding to its gene promoter, we first predicted the putative binding sites of Prrx1 in ABCC1 pro-

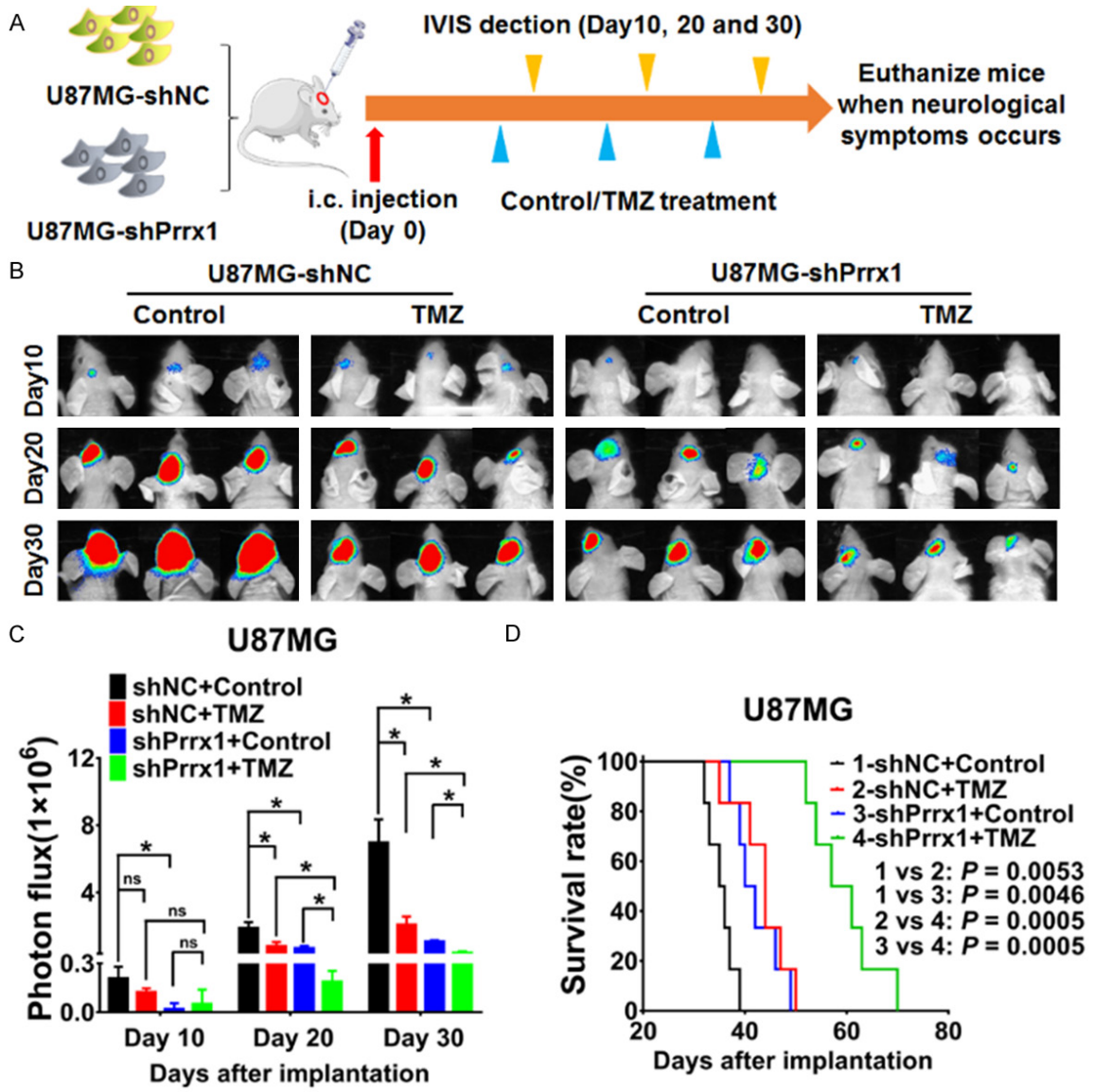

Figure 2. Silencing Prrx1 increased the sensitivity of TMZ on glioma cells *in vivo*. (A) Schematic diagram showing TMZ treatment of U87-shNC- and U87-shPrrx1-derived xenograft. (B, C) In vivo bioluminescent images (B) and the quantification (C) of xenograft-bearing mice with the indicated treatment at the indicated time points. (D) Kaplan-Meier survival analysis of xenograft-bearing mice with indicated treatment. n = 6 for each group. *$P < 0.05$.

moter by using the bioinformatics algorithm JASPAR, and the results showed that the ABCC1 promoter contained eight different sequences that could act as binding sites for Prrx1 (Supplementary Table 1). Among them, the top two potential binding sites (site 1 and 2) were chosen for subsequent studies. Luciferase reporter assays demonstrated that Prrx1 could bind to both site 1 and 2 in 293T and LN229 cells (**Figure 4F**). More importantly, ChIP assay also verified that both site 1 and site 2 could serve as the binding site for Prrx1 in LN229 and U251 cells (**Figure 4G**). Moreover, to determine whether Prrx1 mediated TMZ resistance through upregulating ABCC1, we performed rescue experiments in which ABCC1 was silenced by siRNA. Transient transfection of siABCC1 in Prrx1-overexpressing LN229 cells markedly attenuated Prrx1-mediated TMZ resistance. Specifically, the IC50 value of TMZ for Prrx1-overexpressed LN229 cells was 373.4 μM, but this value was decreased to 285.0 μM when LN229 cells were transiently transfected with siABCC1 (**Figure 4H**). Similar effect of siABCC1

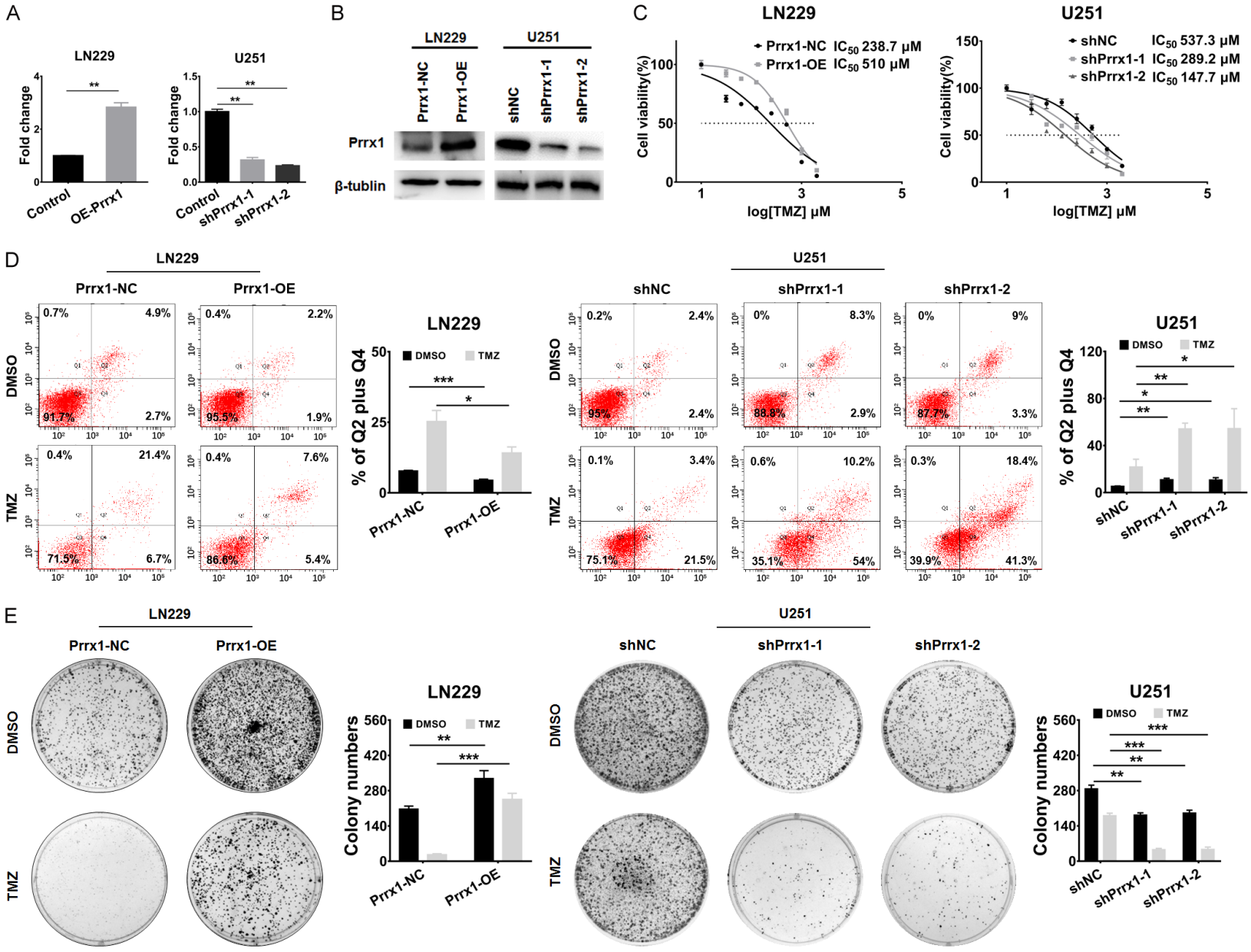
A
LN229
U251
Fold change
Control
OE-Prrx1
shPrrx1-1
shPrrx1-2
B
LN229
U251
Prrx1-NC
Prrx1-OE
shNC
shPrrx1-1
shPrrx1-2
Prrx1
β-tublin
C
LN229
Prrx1-NC IC50 238.7 μM
Prrx1-OE IC50 510 μM
Cell viability(%)
log[TMZ] μM
U251
shNC IC50 537.3 μM
shPrrx1-1 IC50 289.2 μM
shPrrx1-2 IC50 147.7 μM
D
LN229
Prrx1-NC
Prrx1-OE
DMSO
TMZ
0.7%
4.9%
91.7%
2.7%
0.4%
2.2%
95.5%
1.9%
0.4%
21.4%
71.5%
6.7%
0.4%
7.6%
86.6%
5.4%
% of Q2 plus Q4
U251
shNC
shPrrx1-1
shPrrx1-2
0.2%
2.4%
95%
2.4%
0%
8.3%
88.8%
2.9%
0%
9%
87.7%
3.3%
0.1%
3.4%
75.1%
21.5%
0.6%
10.2%
35.1%
54%
0.3%
18.4%
39.9%
41.3%
E
LN229
Prrx1-NC
Prrx1-OE
DMSO
TMZ
Colony numbers
U251
shNC
shPrrx1-1
shPrrx1-2

Figure 3. Silencing Prrx1 increased the sensitivity of TMZ on glioma cells *in vitro*. (A, B) RT-qPCR (A) and western blot (B) assays were used to verify the successful construction of Prrx1 overexpression (left panel) and knockdown (right panel) glioma cells. (C) The cell viability was determined by CCK-8 assays. LN229 (left panel) and U251 (right panel) cells were exposed to TMZ over the range of 0-2000 μM for 48 h followed by IC50 analysis. (D) Analysis of cell apoptosis by Annexin V-PE/7-AAD staining in LN229 cells and Annexin V-APC/7-AAD staining in U251 cells after indicated treatment. n = 3 for each group. (E) Analysis of cell sensitivity to TMZ by crystal violet staining after indicated treatment. n = 3 for each group. *P < 0.05, **P < 0.01, ***P < 0.001.

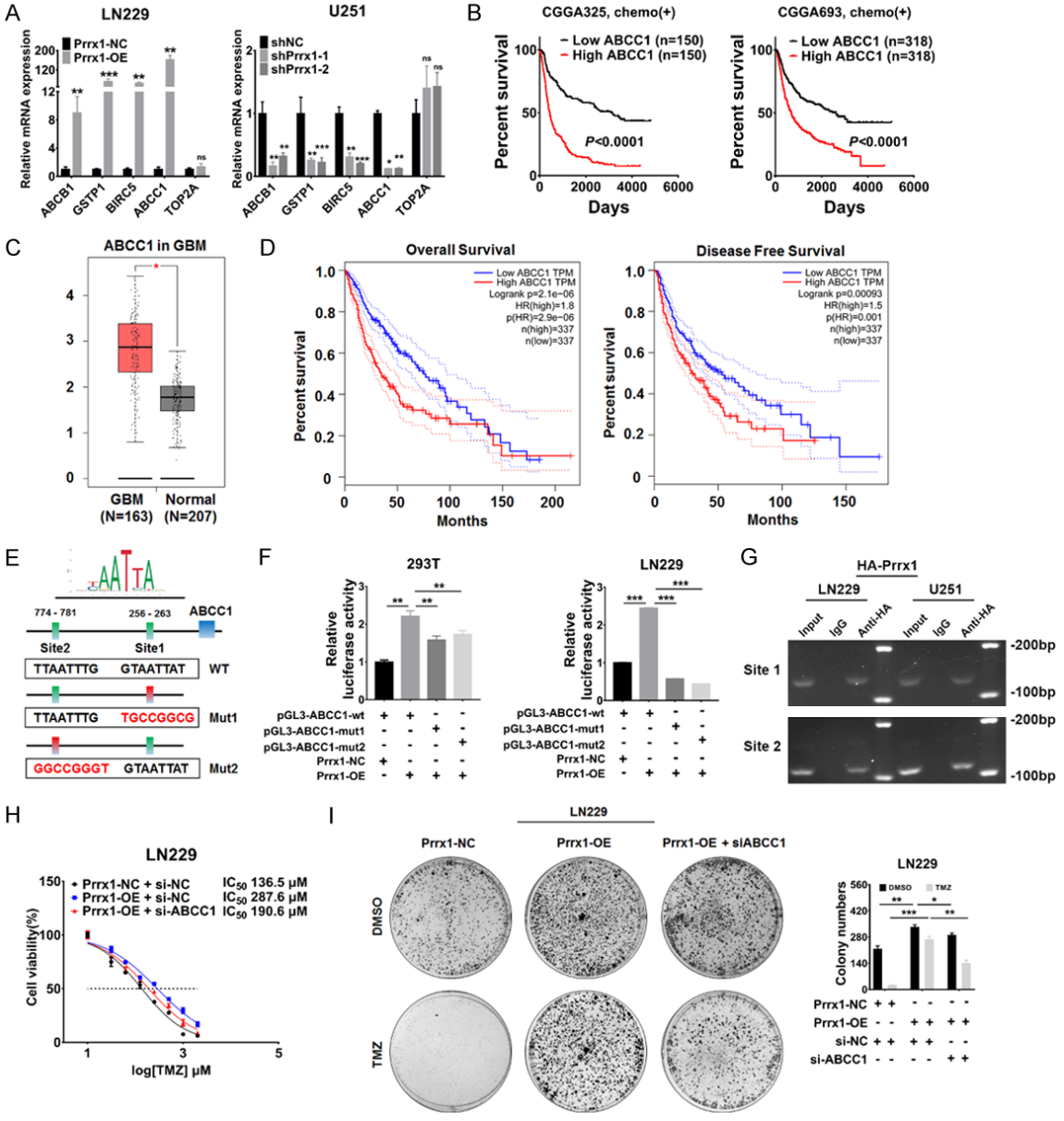

Figure 4. The critical role of ABCC1 upregulation in Prrx1-mediated resistance to TMZ. (A) RT-qPCR detected the effect of Prrx1 on the expression of MDR genes in LN229 (left panel) and U251 (right panel) cells (mean ± SD, n = 3). (B) Survival curves of chemo-treated glioma patients with distinct ABCC1 expression level from the CGGA database. (C) Transcriptional expression of ABCC1 in GBM relative to normal brain tissues (GEPIA database). (D) Overall survival (left panel) and disease-free survival (right panel) curve comparison between the high and low expression of ABCC1 (determined by the quantile value) for the TCGA glioma patient cohort. (E) Potential binding sites of Prrx1 in ABCC1 promotor were predicted by JASPAR2020 (http://jaspar.genereg.net). (F) ABCC1 wild type or mutant luciferase reporters were co-transfected with pwslv-07-Prrx1, and luciferase reporter assays were performed. (G) Amplification of Prrx1-binding sites 1 and 2 after ChIP analysis using anti-HA antibody was indicated in the PCR gel. The gel figures were accompanied by the locations of molecular weight markers. (H, I) Effects of ABCC1 siRNA on Prrx1-induced resistance to TMZ by CCK-8 assay (H) and crystal violet staining (I). *P < 0.05, **P < 0.01, ***P < 0.001.

on Prrx1-mediated colony formation was observed (**Figure 4I**). Collectively, these results indicate that Prrx1 transactivates ABCC1 via direct binding to its promoter region, which, in turn, causes TMZ resistance.

Prrx1 promoted GSCs-based VM formation both in vitro and in vivo

It is well known that not only the intrinsic elevated MDR genes expression, but also the extrinsic vascular microenvironment contributes to the acquired resistance of glioma cells to TMZ. Aberrant vessels around the glioma obstruct the delivery and distribution of chemotherapeutics, which eventually leads to chemoresistance. We previously reported that Prrx1 promoted glioma stemness and angiogenesis via activating TGF-β/Smad pathway and upregulating proangiogenic factors [20]. Herein, we aimed to explored whether Prrx1 induced TMZ resistance by regulating the extrinsic vascular microenvironment. DEG analyses were first performed between $Prrx1^{high}$ and $Prrx1^{low}$ glioma samples from TCGA and CGGA databases (**Figure 5A**, **5B**, Supplementary Figure 1A). Gene ontology (GO) enrichment analyses were then conducted by using the up-regulated genes. The results showed that the DEGs were mainly enriched in cytokines- and extracellular matrix (ECM)-related responses. GSEA analyses of TCGA (**Table 3**), CGGA693 (Supplementary Table 2) and GSE13041 (Supplementary Table 3) datasets further verified the above results. Given the critical roles of Prrx1 in glioma stemness and angiogenesis, it is conceivable that glioma vasculogenic mimicry (VM), a vascular-like structure lined by GSCs independent of the classical angiogenesis, is important for the development of chemoresistance, VM is formed as the result of the plasticity of malignant tumor cells, the remodeling of the extracellular matrix, and the connection of VM channels to the host microcirculation system. Hence, we examined the tube formation, migration, and invasion of glioma cells to assess the effect of Prrx1 expression on VM formation in vitro. The results showed that Prrx1-overexpressed LN229 cells tended to form more vascular-like tubes on Matrigel and displayed stronger migration and invasion properties compared to the control cells. In contrast, suppression of Prrx1 markedly inhibited VM formation of U251 cells (**Figure 5C**, **5D**, Supplementary Figure 1B). We further determined the effects of Prrx1 on the protein expression of MMP2, MMP9 and CD144, molecules that explicitly correlated with VM formation (**Figure 5E**). The results revealed that overexpressing Prrx1 led to a significant upregulation of CD144, MMP2 and MMP9. Consistently, silencing Prrx1 showed the opposite results. The effect of Prrx1 on VM formation was also analyzed by monitoring the expression of the endothelial cell (EC) marker CD31 and GSC marker SOX2 by immunofluorescence (IF) and RT-qPCR. IF staining showed that CD31 was not detectable in NSTCs under conventional culture, but was detected during VM formation, further indicating the process of GSCs differentiation to ECs during VM formation (**Figure 5F**). Additionally, we observed a gradual increase of CD31 expression and a dynamic decrease in SOX2 expression in glioma cells during VM formation (Supplementary Figure 1C). To further support these results, IHC staining was adopted in xenograft tumor samples to detect the density of VM by CD31/PAS staining, and we found that the VM density was significantly decreased in Prrx1-silenced tumors (**Figure 5G**). In conclusion, Prrx1 plays a critical role in glioma VM formation.

Prrx1 overexpression correlated with the up-regulation of MDR markers and VM markers in glioma specimens

Finally, we performed bioinformatics and IHC analysis to verify the clinical relevance of Prrx1 overexpression along with the indicated TMZ resistance in glioma specimens. In our study, we collected 72 glioma specimens as well as their corresponding clinicopathological data. High and low Prrx1 expressions were detected in 45 and 27 glioma specimens, respectively, by IHC staining. As shown in **Figure 6A**, Prrx1 expression was positively correlated with the expression of ABCC1, SOX2, Ki67 and CD31. In addition, Prrx1 expression was also positively correlated with VM formation in glioma tissues, with 35.6% and 18.5% of the samples showing VM formation in Prrx1-high and Prrx1-low groups, respectively. Consistently, Prrx1 expression levels in multiple datasets (TCGA, CGGA and GEO) were positively correlated with those biomarkers, including ABCC1, MMP2, SOX2 and VEGF-A, that were tightly associated with multi-drug resistance, glioma stemness and VM formation (**Figure 6B**, Supplementary Figure 2). These data further supported the notion that Prrx1 mediates TMZ resistance

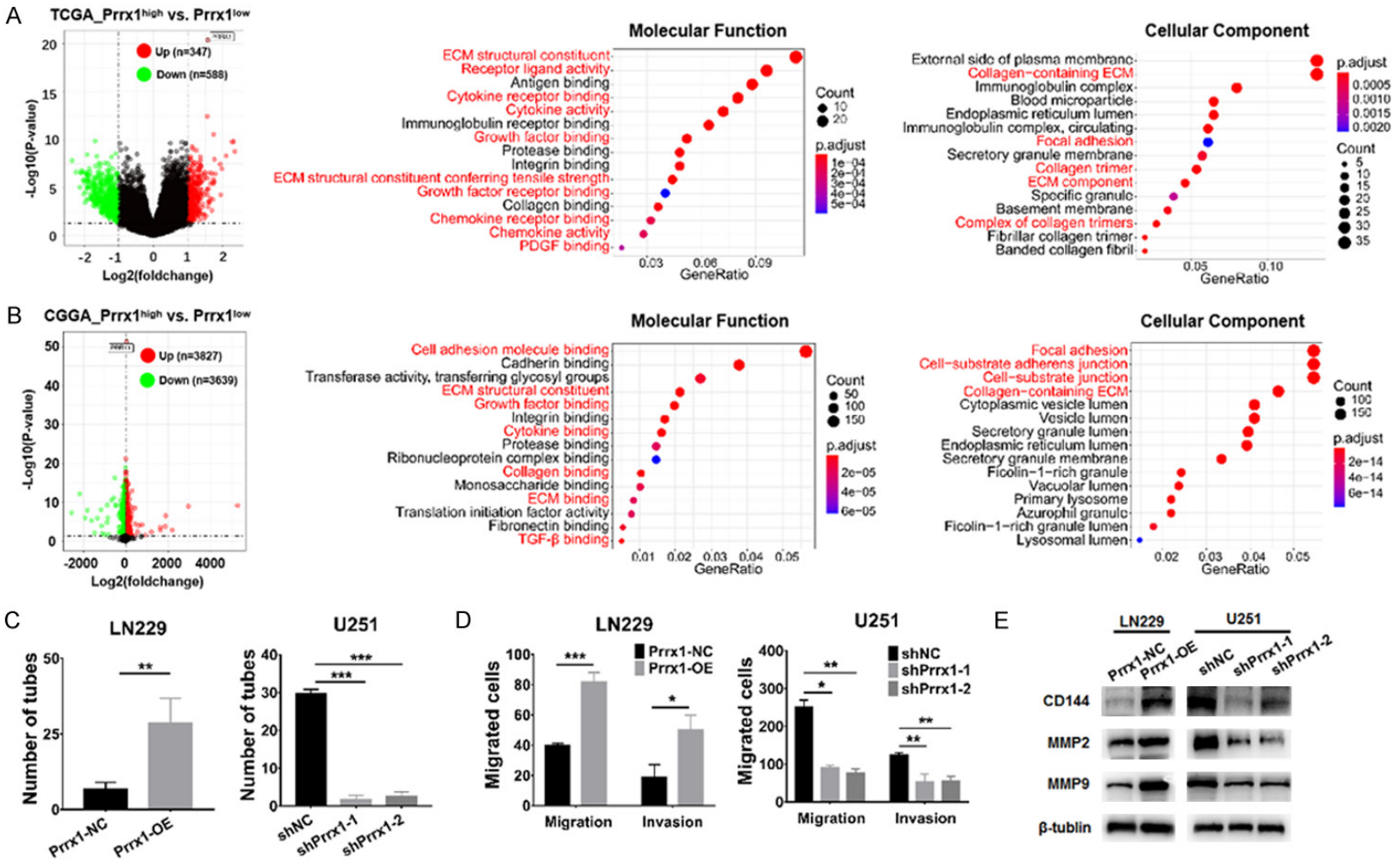
A
TCGA_Prrx1high vs. Prrx1low
Up (n=347)
Down (n=588)
-Log10(P-value)
Log2(foldchange)
Molecular Function
ECM structural constituent
Receptor ligand activity
Antigen binding
Cytokine receptor binding
Cytokine activity
Immunoglobulin receptor binding
Growth factor binding
Protease binding
Integrin binding
ECM structural constituent conferring tensile strength
Growth factor receptor binding
Collagen binding
Chemokine receptor binding
Chemokine activity
PDGF binding
GeneRatio
Count
p.adjust
Cellular Component
External side of plasma membrane
Collagen-containing ECM
Immunoglobulin complex
Blood microparticle
Endoplasmic reticulum lumen
Immunoglobulin complex, circulating
Focal adhesion
Secretory granule membrane
Collagen trimer
ECM component
Specific granule
Basement membrane
Complex of collagen trimers
Fibrillar collagen trimer
Banded collagen fibril
B
CGGA_Prrx1high vs. Prrx1low
Up (n=3827)
Down (n=3639)
-Log10(P-value)
Log2(foldchange)
Molecular Function
Cell adhesion molecule binding
Cadherin binding
Transferase activity, transferring glycosyl groups
ECM structural constituent
Growth factor binding
Integrin binding
Cytokine binding
Protease binding
Ribonucleoprotein complex binding
Collagen binding
Monosaccharide binding
ECM binding
Translation initiation factor activity
Fibronectin binding
TGF-β binding
GeneRatio
Count
p.adjust
Cellular Component
Focal adhesion
Cell-substrate adherens junction
Cell-substrate junction
Collagen-containing ECM
Cytoplasmic vesicle lumen
Vesicle lumen
Secretory granule lumen
Endoplasmic reticulum lumen
Secretory granule membrane
Ficolin-1-rich granule
Vacuolar lumen
Primary lysosome
Azurophil granule
Ficolin-1-rich granule lumen
Lysosomal lumen
GeneRatio
Count
p.adjust
C
LN229
U251
Number of tubes
Prrx1-NC
Prrx1-OE
shNC
shPrrx1-1
shPrrx1-2
D
LN229
U251
Migrated cells
Prrx1-NC
Prrx1-OE
shNC
shPrrx1-1
shPrrx1-2
Migration
Invasion
E
LN229
U251
Prrx1-NC
Prrx1-OE
shNC
shPrrx1-1
shPrrx1-2
CD144
MMP2
MMP9
β-tublin

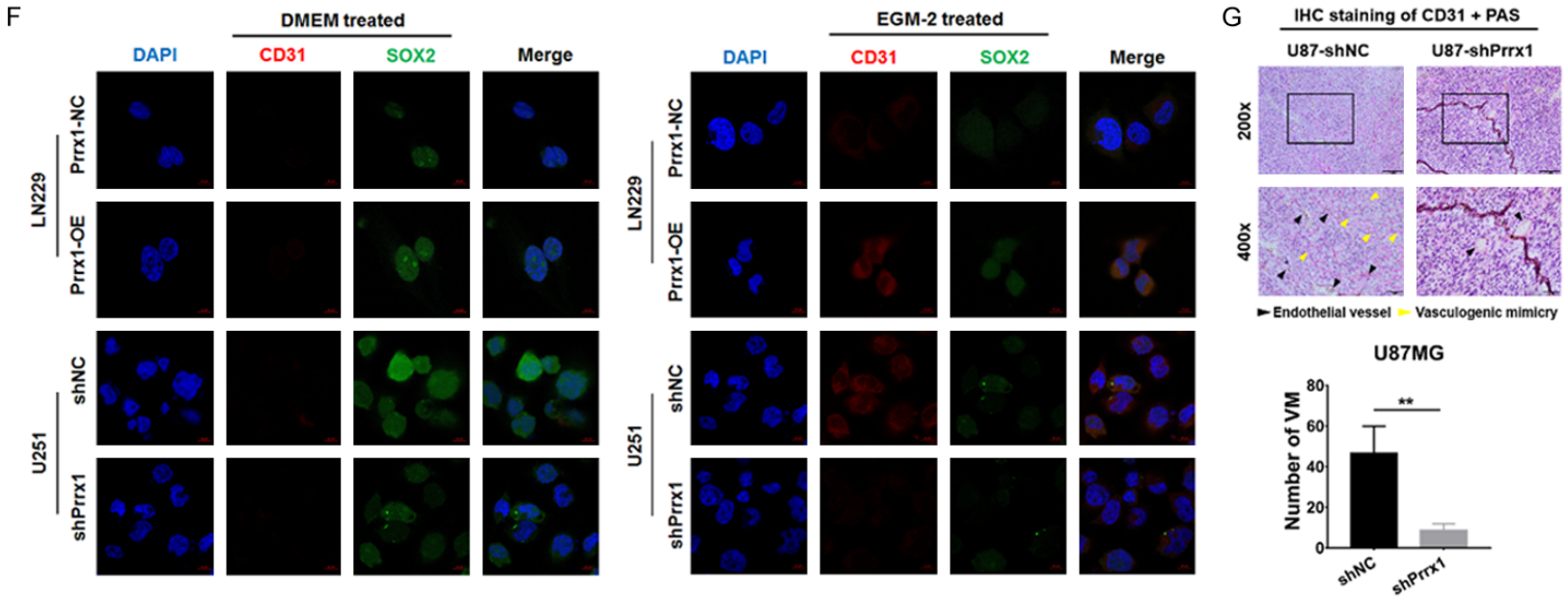

Figure 5. Prrx1 promoted glioma vasculogenic mimicry formation both *in vitro* and *in vivo*. (A, B) The volcano plots on the left represented differential expression between Prrx1^{high} and Prrx1^{low} glioma samples from TCGA (A) and CCGA (B) databases. X-axis indicated the log2 fold-changes (FC) and the Y-axis indicated the negative logarithm to the base 10 of the adjusted *p*-values. Gray vertical and horizontal dashed lines reflected the filtering criteria. Red and green dots represented genes expressed at significantly higher or lower levels, respectively. Top 15 GO enrichment terms (Molecular function and Cellular Component) of up-regulated DEGs from TCGA and CGGA databases were displayed. (C, D) In vitro VM formation assay (above panel) indicated the tube formation ability of cells overexpressing (C) or silencing Prrx1 (D). Transwell assay indicated the migration (middle panel) and invasion (below panel) ability of cells overexpressing (C) or silencing Prrx1 (D). (E) Western blot of CD144, MMP2 and MMP9 in cells overexpressing or silencing Prrx1. (F) IF assay showed the protein levels of SOX2 and CD31 during VM formation in LN229 and U251 cells that were incubated with EGM-2 media to induce VM formation *in vitro*. Scale bar represented 10 μm. (G) VM and EDVs in xenograft tissues were detected and quantified by CD31/PAS staining. Representative images were shown. Scale bar represented 50 μm. **P* < 0.05, ***P* < 0.01, ****P* < 0.001.

Table 3. GSEA results of TCGA GBM cohorts (n = 174)

NAME	NES	NOM p-val	FDR q-val
KEGG_ECM_RECEPTOR_INTERACTION	1.950904	0	0.096702
REACTOME_NON_INTEGRIN_MEMBRANE_ECM_INTERACTIONS	1.947244	0.004264	0.091089
NABA_ECM_REGULATORS	1.932627	0	0.072651
REACTOME_ECM_PROTEOGLYCANS	1.90908	0	0.06501
NABA_ECM_GLYCOPROTEINS	1.794313	0.001972	0.067843
NABA_ECM_AFFILIATED	1.523254	0.029354	0.138633
REACTOME_ACTIVATION_OF_MATRIX_METALLOPROTEINASES	1.537175	0.051173	0.133153
REACTOME_EXTRACELLULAR_MATRIX_ORGANIZATION	2.013989	0	0.170348
REACTOME_DEGRADATION_OF_THE_EXTRACELLULAR_MATRIX	1.803343	0.005882	0.065821
REACTOME_CELL_EXTRACELLULAR_MATRIX_INTERACTIONS	1.564513	0.04142	0.125371
REACTOME_COLLAGEN_FORMATION	1.931622	0	0.069271
REACTOME_ASSEMBLY_OF_COLLAGEN_FIBRILS_AND_OTHER_MULTIMERIC_STRUCTURES	1.899769	0.002058	0.069021
REACTOME_COLLAGEN_BIOSYNTHESIS_AND_MODIFYING_ENZYMES	1.899155	0	0.066498
REACTOME_COLLAGEN_CHAIN_TRIMERIZATION	1.776006	0.003984	0.068756
NABA_COLLAGENS	1.776006	0.003984	0.067984
REACTOME_COLLAGEN_DEGRADATION	1.774017	0.008282	0.067702
REACTOME_PLATELET_ADHESION_TO_EXPOSED_COLLAGEN	1.752779	0.002012	0.074038
REACTOME_CROSSLINKING_OF_COLLAGEN_FIBRILS	1.715786	0.008247	0.075777
KEGG_CYTOKINE_CYTOKINE_RECEPTOR_INTERACTION	1.881549	0.004032	0.062722
SA_MMP_CYTOKINE_CONNECTION	1.769554	0.002101	0.068091
KEGG_CHEMOKINE_SIGNALING_PATHWAY	1.686695	0.041068	0.084441
ANGIOGENESIS	1.742713	0.004073	0.072941
KEGG_RENIN_ANGIOTENSIN_SYSTEM	1.709878	0.021097	0.07684
HU_ANGIOGENESIS_UP	1.582982	0.023762	0.117953
REACTOME_METABOLISM_OF_ANGIOTENSINOGEN_TO_ANGIOTENSINS	1.579418	0.045455	0.119478
PID_VEGFR1_PATHWAY	1.540403	0.045908	0.135013
REACTOME_VEGFR2_MEDIATED_VASCULAR_PERMEABILITY	1.527508	0.038388	0.137947
REACTOME_SIGNALING_BY_VEGF	1.649281	0.027668	0.097903
PID_PDGFRA_PATHWAY	1.555642	0.041584	0.129265
PID_PDGFRB_PATHWAY	1.51414	0.045549	0.141541
REACTOME_SIGNALING_BY_PDGF	1.883464	0	0.063368
PID_ANGIOPOIETIN_RECEPTOR_PATHWAY	1.746296	0.004057	0.074398
KEGG_TGF_BETA_SIGNALING_PATHWAY	1.832051	0	0.063093
REACTOME_SIGNALING_BY_TGF_BETA_FAMILY_MEMBERS	1.702472	0.011834	0.080554
REACTOME_SMAD2_SMAD3:SMAD4_HETEROTRIMER_REGULATES_TRANSCRIPTION	1.598691	0.015625	0.111742
REACTOME_TRANSCRIPTIONAL_ACTIVITY_OF_SMAD2_SMAD3:SMAD4_HETEROTRIMER	1.526447	0.02947	0.138023

through intrinsic MDR and extrinsic VM formation.

Discussion

TMZ is currently the frontline chemotherapeutic reagent for primary and recurrent GBM; however, it shows limited improvement on patient prognosis due to the high therapeutic resistance [21, 22]. Although elevated MGMT expression is widely considered responsible for the intrinsic TMZ resistance, only approximately half of GBMs express MGMT [23, 24], and GBMs with low MGMT expression also display resistance to TMZ therapy [25, 26]. Growing evidence has suggested MDR as an intrinsic MGMT-independent mechanism for TMZ resistance in gliomas. In addition, vascular microenvironment remodeling, such as VM, also contributes to TMZ resistance as extrinsic factors [27]. However, the molecular mechanisms underlying MDR and VM-mediated therapeutic resistance remain to be elucidated. In the present study, we identified the involvement of

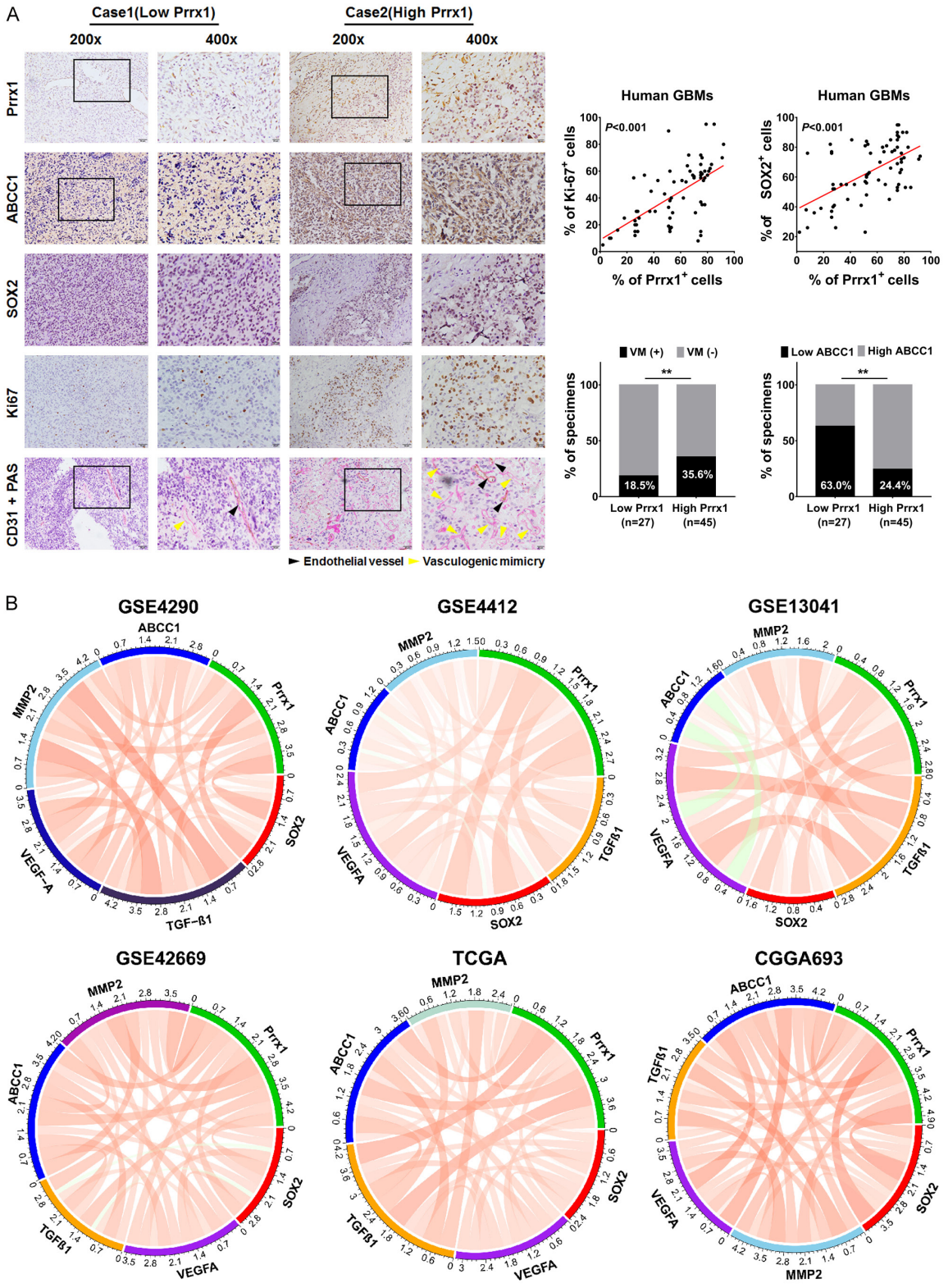

Figure 6. Association in the expression levels between Prrx1 and downstream genes in glioma specimens. A. Prrx1 expression was positively correlated with ABCC1, SOX2, Ki67 expression and the formation of VM in 72 clinical glioma specimens. Two representative cases and percentages of samples showing low or high Prrx1 expression relative to ABCC1, SOX2, Ki67 and VM levels. Scale bar represents 50 μm. B. Circos plot displaying the interconnectivity among genes related to TGF-β/Smad pathway (TGF-β1), stemness (SOX2), vascularization (VEGF-A), extracellular matrix (MMP2) and multi-drug resistance (ABCC1). The thickness and color of the ribbons correlated with the association of genes expression in TCGA, CCGA and multiple GEO datasets.

Prrx1 in TMZ resistance via regulating MDR and VM.

Although diverse mechanisms have been proposed to contribute to MDR, increased ABC transporter activity mediated MDR is one of the most studied mechanisms [4]. Previous studies have discovered an elevated expression of ABCC1, ABCC3 and ABCC4 in TMZ-resistant glioma cells [28, 29]. Furthermore, it has been demonstrated that ABCB1 participates in TMZ resistance and is an independent predictor for TMZ responsiveness [30]. Targeting ABC transporters, such as ABCC1, might be a promising therapeutic strategy for reversing TMZ resistance. However, no ABC inhibitors have been developed successfully for clinical use. Thus, inhibiting the expression of ABCC1 has been proposed as an alternative approach to overcome drug resistance [31]. In our current study, we observed a positive correlation in expression level between Prrx1 and ABCC1 from experimental and clinical data, suggesting that Prrx1 might play a role in TMZ resistance, and that targeting of Prrx1 might be a strategy to overcome TMZ resistance. Indeed, we observed that silencing Prrx1 markedly enhanced the TMZ-mediated cytotoxicity both *in vitro* and *in vivo*. Consistent with our findings, it has been reported that the inhibition of IRE1α RNase activity suppresses the expression of ABCC1 and sensitizes 5-FU-resistant colon cancer cells to drug treatment [8]. Similar study was reported too, in which knockdown of MCAM reduced ABCC1 expression, leading to a remarkable increase in apoptosis after chemotherapy in drug resistant small cell lung cancer [7]. In our study, we also aimed to understand the molecular mechanisms of Prrx1 regulation in ABCC1 expression. By performing CHIP assay and luciferase activity assay, we found that Prrx1 bound to the promoter region of ABCC1 and transactivated its transcription. Clinically, Prrx1 expression was inversely related to overall survival of glioma patients receiving standard of care. Interestingly, we were surprised to observe that only patients with low Prrx1 expression could benefit from chemotherapy, which further demonstrated the important role of Prrx1 in chemoresistance of glioma cells.

Malignant gliomas are characterized by structurally and functionally aberrant vessels that attenuate the delivery of antitumor agents, leading to therapeutic resistance. Conventional antiangiogenic therapies that target the endothelial cells (ECs) have shown limited efficacy in overall survival in both animal models [32, 33] and clinical trials [34, 35], suggesting the existence of an alternative mechanism of escape that bypasses the classical ECs-mediated EDVs. VM, a vascular-like structures formed by highly plastic cancer cells other than ECs, is reported to involve in this mechanism of escape. Several studies have demonstrated the presence of VM and its association with poor prognosis in gliomas [36]. Its formation is associated with three elements: the plasticity of malignant tumor cells, the remodeling of ECMs and the connection of VM channels to the host microcirculation system [37-39]. Our previous study has shown that Prrx1 potentiates the stemness acquisition of non-stem tumor cells (NSTCs) and the stemness maintenance of GSCs in gliomas [20], suggesting the potential role of Prrx1 in VM formation through facilitating the plasticity of glioma cells. The IF and qPCR results in this study further verified its implication in GSCs's transdifferentiation into ECs. Furthermore, GO analyses showed that the functions of Prrx1 were mainly enriched in cytokines- and ECM-related pathways. Consistent with our bioinformatic analyses, we found that Prrx1 markedly upregulated the expression of MMP2, MMP9 and CD144, which is known to promote VM formation via remodeling ECM [40, 41]. Moreover, the positive correlation between the expression of Prrx1 and pro-angiogenic genes, such as VEGF-A and ECM biomarkers MMP2, was also verified in multiple glioma datasets. Clinical data also demonstrated the positive correlation between Prrx1 expression and VM positive rate in glioma specimens. Nevertheless, the precise mechanisms underlying Prrx1 regulation of ECM requires further investigation.

Dysregulation of TGF-β/Smad pathway plays key roles in the pathogenesis of various diseases including gliomas [42]. We have previous revealed that Prrx1 promoted glioma malignant behaviors, including stemness and angiogenesis, via activating TGF-β1 expression and its downstream TGF-β/Smad signaling [20]. TGF-β signaling has recently been shown to regulate chemoresistance in various cancers [43]. For example, TGF-β signaling was reported to contribute to drug resistance in liver cancer cells by inducing the expression of xenobiotic nuclear receptor PXR, thereby leading to increased

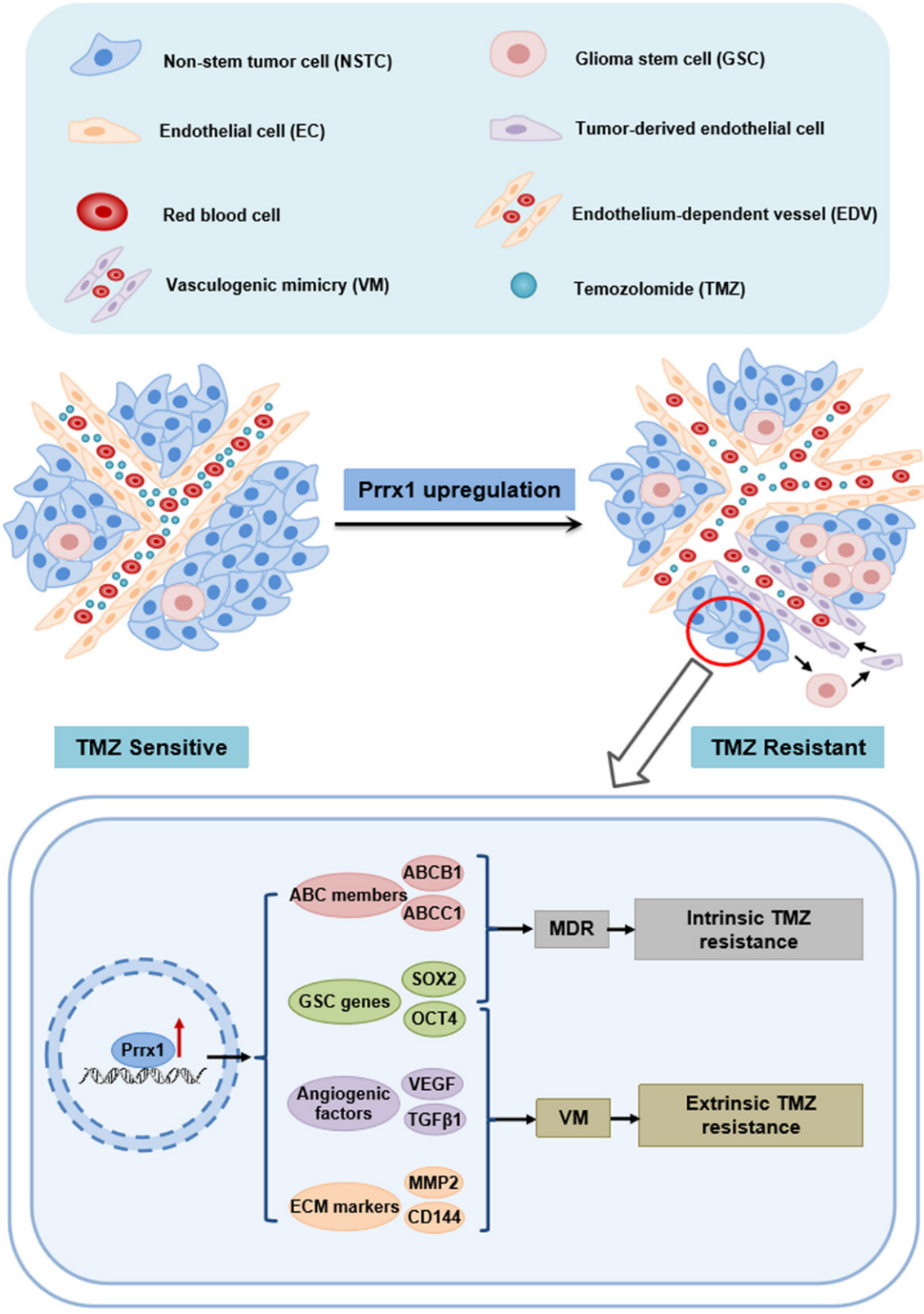

Figure 7. Schematic diagram of the mechanism of Prrx1-mediated TMZ resistance in gliomas.

expression of ABC transporters and reduced apoptosis [44]. Additionally, in ovarian cancer, activation of TGF-β signaling induced osteopontin expression and secretion by mesothelial cells which facilitated ovarian cancer cell chemoresistance via the activation of the CD44 receptor, PI3K/AKT signaling, and ABC transporters [45]. GSCs, which display elevated expression of MDR-related genes, such as ABCB1, ABCC1 and ABCG2, are also recognized to be associated with intrinsic therapeutic resistance to TMZ [46]. Moreover, our and other studies have indicated that TGF-β1 was required for VM formation and could serve as a promising therapeutic target of VM in gliomas [47, 48]. Herein, by employing correlation analyses in multiple glioma datasets including TCGA, CGGA and GEO, we revealed a significant positive association among Prrx1, SOX2 (stemness marker), MMP2 (ECM marker), ABCC1 (MDR marker), VEGF-A (proangiogenic factor) and TGF-β1 (TGF-β signaling trigger). Our findings suggested that these factors might be closely related to and complement each other, forming the regulatory network of Prrx1-mediated TMZ resistance in glioma. Future studies are necessary to validate this notion.

Conclusions

Our study revealed the critical role of Prrx1 in TMZ resistance and identified it as an independent predictor of chemotherapy in gliomas. We further demonstrated that Prrx1 enhanced the expression of drug efflux transporters ABCC1 (intrinsic factor) and VM formation (extrinsic factor), which synergically conferred therapeutic resistance to TMZ in gliomas (**Figure 7**). Silencing Prrx1 markedly enhanced the TMZ-mediated cytotoxicity both *in vitro* and *in vivo*. Therefore, targeting Prrx1 might serve as a feasible strategy to overcome the therapeutic resistance in glioma.

Acknowledgements

We appreciate the effort of the physicians in enrolling patients and thank all the patients involved for allowing us to analyze their clinical data. This work was supported by the National Natural Science Foundation of China (No. 82072762, 81802481), China Postdoctoral Science Foundation funded project (No. 2021M701610), Guangdong Basic and Applied Basic Research Foundation (No. 2020A1515010212) and President Foundation of Zhujiang Hospital, Southern Medical University (No. yzjj2018rc04).

Disclosure of conflict of interest

None.

Abbreviations

TMZ, Temozolomide; Prrx1, Paired-related homeobox 1; VM, Vasculogenic Mimicry; ABCC1, ATP binding cassette subfamily C member 1; GBM, Glioblastoma; MDR, Multiple Drug Resistance; EDV, Endothelium-dependent vessel; EC, Endothelial cell; GSC, Glioma stem cell; NSTC, Non-stem tumor cell.

Address correspondence to: Jihui Wang and Yiquan Ke, The National Key Clinical Specialty, Department of Neurosurgery, Zhujiang Hospital, Southern Medical University, Guangzhou 510282, China. E-mail: 346wangjihui@163.com (JHW); kyquan@smu.edu.cn (YQK); Liang Zhao, Department of Pathology, Nanfang Hospital, Southern Medical University, Guangzhou, China; Department of Pathology, School of Basic Medical Sciences, Southern Medical University, Guangzhou, China. E-mail: liangsmu@foxmail.com

References

[1] Omuro A and DeAngelis LM. Glioblastoma and other malignant gliomas: a clinical review. JAMA 2013; 310: 1842-1850.

[2] Stupp R, Mason WP, van den Bent MJ, Weller M, Fisher B, Taphoorn MJ, Belanger K, Brandes AA, Marosi C, Bogdahn U, Curschmann J, Janzer RC, Ludwin SK, Gorlia T, Allgeier A, Lacombe D, Cairncross JG, Eisenhauer E and Mirimanoff RO; European Organisation for Research and Treatment of Cancer Brain Tumor and Radiotherapy Groups; National Cancer Institute of Canada Clinical Trials Group. Radiotherapy plus concomitant and adjuvant temozolomide for glioblastoma. N Engl J Med 2005; 352: 987-996.

[3] Rabik CA, Njoku MC and Dolan ME. Inactivation of O6-alkylguanine DNA alkyltransferase as a means to enhance chemotherapy. Cancer Treat Rev 2006; 32: 261-276.

[4] Saraswathy M and Gong S. Different strategies to overcome multidrug resistance in cancer. Biotechnol Adv 2013; 31: 1397-1407.

[5] Wu Q, Yang Z, Nie Y, Shi Y and Fan D. Multi-drug resistance in cancer chemotherapeutics: mechanisms and lab approaches. Cancer Lett 2014; 347: 159-166.

[6] Chen Z, Shi T, Zhang L, Zhu P, Deng M, Huang C, Hu T, Jiang L and Li J. Mammalian drug efflux transporters of the ATP binding cassette (ABC) family in multidrug resistance: a review of the past decade. Cancer Lett 2016; 370: 153-164.

[7] Tripathi SC, Fahrmann JF, Celiktas M, Aguilar M, Marini KD, Jolly MK, Katayama H, Wang H, Murage EN, Dennison JB, Watkins DN, Levine H, Ostrin EJ, Taguchi A and Hanash SM. MCAM mediates chemoresistance in small-cell lung cancer via the PI3K/AKT/SOX2 signaling pathway. Cancer Res 2017; 77: 4414-4425.

[8] Gao Q, Li XX, Xu YM, Zhang JZ, Rong SD, Qin YQ and Fang J. IRE1α-targeting downregulates ABC transporters and overcomes drug resistance of colon cancer cells. Cancer Lett 2020; 476: 67-74.

[9] Xiao Q, Zhou Y, Winter S, Büttner F, Schaeffeler E, Schwab M and Lauschke VM. Germline variant burden in multidrug resistance transporters is a therapy-specific predictor of survival in breast cancer patients. Int J Cancer 2020; 146: 2475-2487.

[10] Deeley RG, Westlake C and Cole SP. Transmembrane transport of endo- and xenobiotics by mammalian ATP-binding cassette multidrug resistance proteins. Physiol Rev 2006; 86: 849-899.

[11] Pajic M, Murray J, Marshall GM, Cole SP, Norris MD and Haber M. ABCC1 G2012T single nucleotide polymorphism is associated with patient outcome in primary neuroblastoma and altered stability of the ABCC1 gene transcript. Pharmacogenet Genomics 2011; 21: 270-279.

[12] Haber M, Smith J, Bordow SB, Flemming C, Cohn SL, London WB, Marshall GM and Norris MD. Association of high-level MRP1 expression with poor clinical outcome in a large prospective study of primary neuroblastoma. J Clin Oncol 2006; 24: 1546-1553.

[13] Norden AD, Drappatz J and Wen PY. Novel antiangiogenic therapies for malignant gliomas. Lancet Neurol 2008; 7: 1152-1160.

[14] Khasraw M, Ameratunga MS, Grant R, Wheeler H and Pavlakis N. Antiangiogenic therapy for high-grade glioma. Cochrane Database Syst Rev 2014; CD008218.

[15] Field KM, Jordan JT, Wen PY, Rosenthal MA and Reardon DA. Bevacizumab and glioblastoma: scientific review, newly reported updates, and ongoing controversies. Cancer 2015; 121: 997-1007.

[16] Lai A, Tran A, Nghiemphu PL, Pope WB, Solis OE, Selch M, Filka E, Yong WH, Mischel PS, Liau LM, Phuphanich S, Black K, Peak S, Green RM, Spier CE, Kolevska T, Polikoff J, Fehrenbacher L, Elashoff R and Cloughesy T. Phase II study of bevacizumab plus temozolomide during and after radiation therapy for patients with newly diagnosed glioblastoma multiforme. J Clin Oncol 2011; 29: 142-148.

[17] Li Y, Wang W, Wang F, Wu Q, Li W, Zhong X, Tian K, Zeng T, Gao L, Liu Y, Li S, Jiang X, Du G and Zhou Y. Paired related homeobox 1 transactivates dopamine D2 receptor to maintain propagation and tumorigenicity of glioma-initiating cells. J Mol Cell Biol 2017; 9: 302-314.

[18] Sugiyama M, Hasegawa H, Ito S, Sugiyama K, Maeda M, Aoki K, Wakabayashi T, Hamaguchi M, Natsume A and Senga T. Paired related homeobox 1 is associated with the invasive properties of glioblastoma cells. Oncol Rep 2015; 33: 1123-1130.

[19] Maniotis AJ, Folberg R, Hess A, Seftor EA, Gardner LM, Pe'er J, Trent JM, Meltzer PS and Hendrix MJ. Vascular channel formation by human melanoma cells in vivo and in vitro: vasculogenic mimicry. Am J Pathol 1999; 155: 739-752.

[20] Chen Z, Chen Y, Li Y, Lian W, Zheng K, Zhang Y, Zhang Y, Lin C, Liu C, Sun F, Sun X, Wang J, Zhao L and Ke Y. Prrx1 promotes stemness and angiogenesis via activating TGF-beta/smad pathway and upregulating proangiogenic factors in glioma. Cell Death Dis 2021; 12: 615.

[21] Stupp R, Hegi ME, Mason WP, van den Bent MJ, Taphoorn MJ, Janzer RC, Ludwin SK, Allgeier A, Fisher B, Belanger K, Hau P, Brandes AA, Gijtenbeek J, Marosi C, Vecht CJ, Mokhtari K, Wesseling P, Villa S, Eisenhauer E, Gorlia T, Weller M, Lacombe D, Cairncross JG and Mirimanoff RO. Effects of radiotherapy with concomitant and adjuvant temozolomide versus radiotherapy alone on survival in glioblastoma in a randomised phase III study: 5-year analysis of the EORTC-NCIC trial. Lancet Oncol 2009; 10: 459-466.

[22] Van Meir EG, Hadjipanayis CG, Norden AD, Shu HK, Wen PY and Olson JJ. Exciting new advances in neuro-oncology: the avenue to a cure for malignant glioma. CA Cancer J Clin 2010; 60: 166-193.

[23] Brennan CW, Verhaak RG, McKenna A, Campos B, Noushmehr H, Salama SR, Zheng S, Chakravarty D, Sanborn JZ, Berman SH, Beroukhim R, Bernard B, Wu CJ, Genovese G, Shmulevich I, Barnholtz-Sloan J, Zou L, Vegesna R, Shukla SA, Ciriello G, Yung WK, Zhang W, Sougnez C, Mikkelsen T, Aldape K, Bigner DD, Van Meir EG, Prados M, Sloan A, Black KL, Eschbacher J, Finocchiaro G, Friedman W, Andrews DW, Guha A, Iacocca M, O'Neill BP, Foltz G, Myers J, Weisenberger DJ, Penny R, Kucherlapati R, Perou CM, Hayes DN, Gibbs R, Marra M, Mills GB, Lander E, Spellman P, Wilson R,

Sander C, Weinstein J, Meyerson M, Gabriel S, Laird PW, Haussler D, Getz G, Chin L and Network TR. The somatic genomic landscape of glioblastoma. Cell 2013; 155: 462-477.

[24] Hegi ME, Diserens AC, Gorlia T, Hamou MF, de Tribolet N, Weller M, Kros JM, Hainfellner JA, Mason W, Mariani L, Bromberg JE, Hau P, Mirimanoff RO, Cairncross JG, Janzer RC and Stupp R. MGMT gene silencing and benefit from temozolomide in glioblastoma. N Engl J Med 2005; 352: 997-1003.

[25] Agnihotri S, Burrell K, Buczkowicz P, Remke M, Golbourn B, Chornenkyy Y, Gajadhar A, Fernandez NA, Clarke ID, Barszczyk MS, Pajovic S, Ternamian C, Head R, Sabha N, Sobol RW, Taylor MD, Rutka JT, Jones C, Dirks PB, Zadeh G and Hawkins C. ATM regulates 3-methylpurine-DNA glycosylase and promotes therapeutic resistance to alkylating agents. Cancer Discov 2014; 4: 1198-1213.

[26] Sarkaria JN, Kitange GJ, James CD, Plummer R, Calvert H, Weller M and Wick W. Mechanisms of chemoresistance to alkylating agents in malignant glioma. Clin Cancer Res 2008; 14: 2900-2908.

[27] Kirschmann DA, Seftor EA, Hardy KM, Seftor RE and Hendrix MJ. Molecular pathways: vasculogenic mimicry in tumor cells: diagnostic and therapeutic implications. Clin Cancer Res 2012; 18: 2726-2732.

[28] Bronger H, König J, Kopplow K, Steiner HH, Ahmadi R, Herold-Mende C, Keppler D and Nies AT. ABCC drug efflux pumps and organic anion uptake transporters in human gliomas and the blood-tumor barrier. Cancer Res 2005; 65: 11419-11428.

[29] de Faria GP, de Oliveira JA, de Oliveira JG, Romano Sde O, Neto VM and Maia RC. Differences in the expression pattern of P-glycoprotein and MRP1 in low-grade and high-grade gliomas. Cancer Invest 2008; 26: 883-889.

[30] Schaich M, Kestel L, Pfirrmann M, Robel K, Illmer T, Kramer M, Dill C, Ehninger G, Schackert G and Krex D. A MDR1 (ABCB1) gene single nucleotide polymorphism predicts outcome of temozolomide treatment in glioblastoma patients. Ann Oncol 2009; 20: 175-181.

[31] Cole SP. Targeting multidrug resistance protein 1 (MRP1, ABCC1): past, present, and future. Annu Rev Pharmacol Toxicol 2014; 54: 95-117.

[32] Ebos JM, Lee CR, Cruz-Munoz W, Bjarnason GA, Christensen JG and Kerbel RS. Accelerated metastasis after short-term treatment with a potent inhibitor of tumor angiogenesis. Cancer Cell 2009; 15: 232-239.

[33] Pàez-Ribes M, Allen E, Hudock J, Takeda T, Okuyama H, Viñals F, Inoue M, Bergers G, Hanahan D and Casanovas O. Antiangiogenic therapy elicits malignant progression of tumors to increased local invasion and distant metastasis. Cancer Cell 2009; 15: 220-231.

[34] Bergers G and Hanahan D. Modes of resistance to anti-angiogenic therapy. Nat Rev Cancer 2008; 8: 592-603.

[35] Ellis LM and Hicklin DJ. VEGF-targeted therapy: mechanisms of anti-tumour activity. Nat Rev Cancer 2008; 8: 579-591.

[36] Mei X, Chen YS, Chen FR, Xi SY and Chen ZP. Glioblastoma stem cell differentiation into endothelial cells evidenced through live-cell imaging. Neuro Oncol 2017; 19: 1109-1118.

[37] Chen YS and Chen ZP. Vasculogenic mimicry: a novel target for glioma therapy. Chin J Cancer 2014; 33: 74-79.

[38] Xu J, Yang X, Deng Q, Yang C, Wang D, Jiang G, Yao X, He X, Ding J, Qiang J, Tu J, Zhang R, Lei QY, Shao ZM, Bian X, Hu R, Zhang L and Liu S. TEM8 marks neovasculogenic tumor-initiating cells in triple-negative breast cancer. Nat Commun 2021; 12: 4413.

[39] Shi Y, Chen C, Zhang X, Liu Q, Xu JL, Zhang HR, Yao XH, Jiang T, He ZC, Ren Y, Cui W, Xu C, Liu L, Cui YH, Yu SZ, Ping YF and Bian XW. Primate-specific miR-663 functions as a tumor suppressor by targeting PIK3CD and predicts the prognosis of human glioblastoma. Clin Cancer Res 2014; 20: 1803-1813.

[40] Liang X, Sun R, Zhao X, Zhang Y, Gu Q, Dong X, Zhang D, Sun J and Sun B. Rictor regulates the vasculogenic mimicry of melanoma via the AKT-MMP-2/9 pathway. J Cell Mol Med 2017; 21: 3579-3591.

[41] Liu Y, Li F, Yang YT, Xu XD, Chen JS, Chen TLA-Ohoo, Chen HJ, Zhu YB, Lin JY, Li Y, Xie XM, Sun XL and Ke YQ. IGFBP2 promotes vasculogenic mimicry formation via regulating CD144 and MMP2 expression in glioma. Oncogene 2019; 38: 1815-1831.

[42] Colak S and Ten Dijke P. Targeting TGF-beta signaling in cancer. Trends Cancer 2017; 3: 56-71.

[43] Brunen D, Willems SM, Kellner U, Midgley R, Simon I and Bernards R. TGF-β: an emerging player in drug resistance. Cell Cycle 2013; 12: 2960-2968.

[44] Bhagyaraj E, Ahuja N, Kumar S, Tiwari D, Gupta S, Nanduri R and Gupta P. TGF-β induced chemoresistance in liver cancer is modulated by xenobiotic nuclear receptor PXR. Cell Cycle 2019; 18: 3589-3602.

[45] Qian J, LeSavage BL, Hubka KM, Ma C, Natarajan S, Eggold JT, Xiao Y, Fuh KC, Krishnan V, Enejder A, Heilshorn SC, Dorigo O and Rankin EB. Cancer-associated mesothelial cells promote ovarian cancer chemoresistance through paracrine osteopontin signaling. J Clin Invest 2021; 131: e146186.

[46] Uribe D, Torres Á, Rocha JD, Niechi I, Oyarzún C, Sobrevia L, San Martín R and Quezada C. Multidrug resistance in glioblastoma stem-like cells: role of the hypoxic microenvironment and adenosine signaling. Mol Aspects Med 2017; 55: 140-151.

[47] Ling G, Wang S, Song Z, Sun X, Liu Y, Jiang X, Cai Y, Du M and Ke Y. Transforming growth factor-β is required for vasculogenic mimicry formation in glioma cell line U251MG. Cancer Biol Ther 2011; 12: 978-988.

[48] Zhang C, Chen W, Zhang X, Huang B, Chen A, He Y, Wang J and Li X. Galunisertib inhibits glioma vasculogenic mimicry formation induced by astrocytes. Sci Rep 2016; 6: 23056.

[49] Wang J, Yang Y, Zhang Y, Huang M, Zhou Z, Luo W, Tang J, Wang J, Xiao Q, Chen H, Cai Y, Sun X, Wang Y and Ke Y. Dual-targeting heparin-based nanoparticles that re-assemble in blood for glioma therapy through both anti-proliferation and anti-angiogenesis. Adv Funct Mater 2016; 26: 7873-7885.

Supplementary Table 1. Potential binding sites of Prrx1 in ABCC1 promoter

Gene	Start	End	Relative Score	Strand	TFBs
ABCC1	256	263	0.940504	-	ATAATTAC
ABCC1	256	263	0.937634	+	GTAATTAT
ABCC1	774	781	0.936916	-	CAAATTAA
ABCC1	834	841	0.90744	-	AAAATTAA
ABCC1	366	373	0.906965	-	CCAATCAA
ABCC1	57	64	0.898895	-	TTAATCAA
ABCC1	1004	1011	0.892401	-	AAAATTAG
ABCC1	57	64	0.889286	+	TTGATTAA
ABCC1	299	306	0.884842	+	CCAATAAA
ABCC1	1108	1115	0.884535	-	GTAATCAA

Supplementary Table 2. GSEA results of CGGA cohorts (n = 693)

NAME	NES	NOM p-val	FDR q-val
REACTOME_NON_INTEGRIN_MEMBRANE_ECM_INTERACTIONS	1.756231	0.017857144	0.11312888
REACTOME_ECM_PROTEOGLYCANS	1.7352844	0.026871402	0.11564275
BIOCARTA_ECM_PATHWAY	1.6180406	0.030991735	0.1352021
NABA_ECM_REGULATORS	1.5551183	0.050301813	0.15848662
REACTOME_CELL_EXTRACELLULAR_MATRIX_INTERACTIONS	1.8902702	0.001949318	0.100156225
REACTOME_EXTRACELLULAR_MATRIX_ORGANIZATION	1.7274162	0.01953125	0.11756934
KEGG_CYTOKINE_CYTOKINE_RECEPTOR_INTERACTION	1.6852491	0.036072146	0.12553535
WP_ANGIOGENESIS	1.6400998	0.035490606	0.13058539
PID_ANGIOPOIETIN_RECEPTOR_PATHWAY	1.8018621	0.008016032	0.1027165
BIOCARTA_VEGF_PATHWAY	1.75773	0.00990099	0.11503212
PID_VEGFR1_2_PATHWAY	1.6675469	0.022680413	0.13136409
PID_PDGFRA_PATHWAY	1.882278	0.004065041	0.09573958
REACTOME_SIGNALING_BY_PDGF	1.816011	0.008080808	0.10182681
PID_PDGFRB_PATHWAY	1.7305127	0.020618556	0.11648043
REACTOME_SIGNALING_BY_TGF_BETA_RECEPTOR_COMPLEX	1.7601182	0.011538462	0.11393335
BIOCARTA_TGFB_PATHWAY	1.578885	0.036093418	0.15207855
REACTOME_TGF_BETA_RECEPTOR_SIGNALING_ACTIVATES_SMADS	1.5689999	0.03522505	0.15684271
KEGG_TGF_BETA_SIGNALING_PATHWAY	2.1022248	0	0.06345833
PID_TGFBR_PATHWAY	1.8953773	0	0.1016302
REACTOME_SIGNALING_BY_TGF_BETA_FAMILY_MEMBERS	1.8378536	0.002004008	0.09734994
PID_SMAD2_3NUCLEAR_PATHWAY	1.9256155	0.001923077	0.096384674
REACTOME_SMAD2_SMAD3:SMAD4_HETEROTRIMER_REGULATES_TRANSCRIPTION	1.7854505	0.001992032	0.10944934
REACTOME_TRANSCRIPTIONAL_ACTIVITY_OF_SMAD2_SMAD3:SMAD4_HETEROTRIMER	1.7484576	0.005859375	0.1122866
REACTOME_TGF_BETA_RECEPTOR_SIGNALING_ACTIVATES_SMADS	1.5689999	0.03522505	0.15684271

Supplementary Table 3. GSEA results of GSE13041-GPL96 cohorts (n = 181)

NAME	NES	NOM p-val	FDR q-val
REACTOME_NON_INTEGRIN_MEMBRANE_ECM_INTERACTIONS	1.642888	0.024390243	0.12733296
REACTOME_ECM_PROTEOGLYCANS	1.6387221	0.03992016	0.13041192
BIOCARTA_ECM_PATHWAY	1.4809289	0.05284553	0.23115532
REACTOME_CELL_EXTRACELLULAR_MATRIX_INTERACTIONS	1.7268853	0.016096579	0.09281693
REACTOME_EXTRACELLULAR_MATRIX_ORGANIZATION	1.6594485	0.030120483	0.115392365
REACTOME_DEGRADATION_OF_THE_EXTRACELLULAR_MATRIX	1.5589839	0.044715445	0.18118568
PID_ANGIOPOIETIN_RECEPTOR_PATHWAY	1.5702149	0.03125	0.17170212
BIOCARTA_VEGF_PATHWAY	1.558939	0.03327172	0.18032628
REACTOME_SIGNALING_BY_VEGF	1.505494	0.047227927	0.21297327
PID_VEGFR1_2_PATHWAY	1.489891	0.048879836	0.2231679
PID_PDGFRA_PATHWAY	1.8369184	0.007968128	0.057295475
PID_PDGFRB_PATHWAY	1.6594565	0.01622718	0.11620921
REACTOME_SIGNALING_BY_PDGF	1.6534648	0.026476579	0.119179815
BIOCARTA_PDGF_PATHWAY	1.5908468	0.033009708	0.15496147
BIOCARTA_TGFB_PATHWAY	1.9144677	0	0.043166604
KEGG_TGF_BETA_SIGNALING_PATHWAY	1.8863064	0.002083333	0.04028972
PID_TGFBR_PATHWAY	1.7813516	0	0.07325195
REACTOME_SIGNALING_BY_TGF_BETA_RECEPTOR_COMPLEX	1.5289905	0.036363635	0.19652732
REACTOME_SIGNALING_BY_TGF_BETA_FAMILY_MEMBERS	1.4594214	0.047325104	0.25090826
PID_SMAD2_3PATHWAY	1.7796818	0.006048387	0.07119367
REACTOME_SMAD2_SMAD3:SMAD4_HETEROTRIMER_REGULATES_TRANSCRIPTION	1.6875771	0.016	0.107613936
REACTOME_TRANSCRIPTIONAL_ACTIVITY_OF_SMAD2_SMAD3:SMAD4_HETEROTRIMER	1.6006551	0.001992032	0.14766191
PID_SMAD2_3NUCLEAR_PATHWAY	1.9387324	0	0.043517027

Supplementary Table 4. RT-qPCR primer sequences for human genes

Gene	Forward primer	Reverse primer	Product length
Prrx1	TGATGCTTTTGTGCGAGAAGA	AGGGAAGCGTTTTTATTGGCT	135 bp
GAPDH	GGAGCGAGATCCCTCCAAAAT	GGCTGTTGTCATACTTCTCATGG	197 bp
ABCB1	TTGCTGCTTACATTCAGGTTTCA	AGCCTATCTCCTGTCGCATTA	105 bp
GSTP1	CCCTACACCGTGGTCTATTTCC	CAGGAGGCTTTGAGTGAGC	137 bp
BIRC5	AGGACCACCGCATCTCTACAT	AAGTCTGGCTCGTTCTCAGTG	118 bp
ABCC1	TTACTCATTCAGCTCGTCTTGTC	CAGGGATTAGGGTCGTGGAT	80 bp
TOP2A	ACCATTGCAGCCTGTAAATGA	GGGCGGAGCAAAATATGTTCC	129 bp

Supplementary Table 5. PCR primer sequences

Primer name	Forward primer sequence	Reverse primer sequence	Product length
Site 1	GCCTTAGTGGCCTCATC	CTGGGCAACAGAGCAA	185 bp
Site 2	AACAGCATAACTGGCATTA	AGGACCTAGCGAGGGA	139 bp

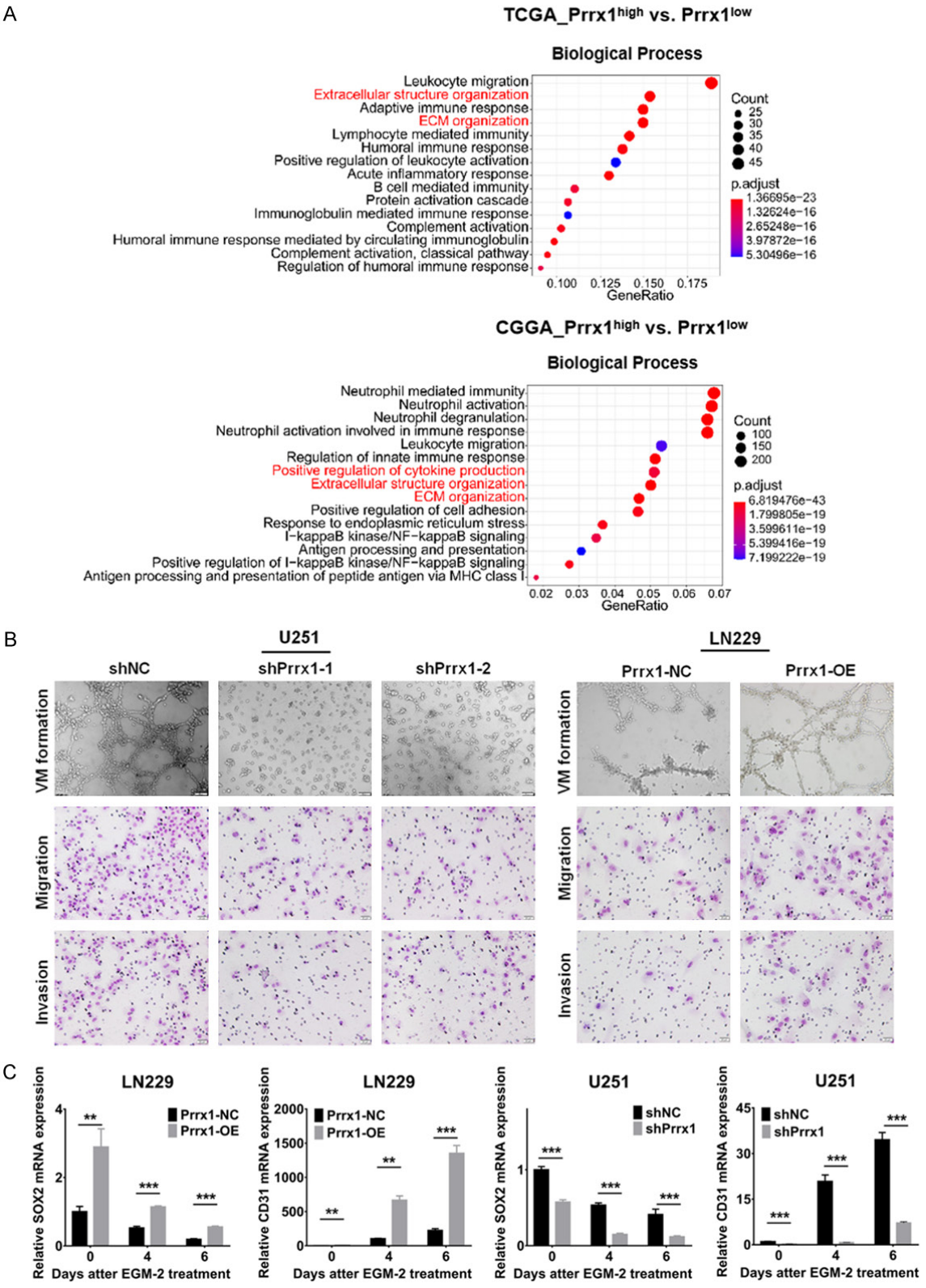

Supplementary Figure 1. A. Top 15 GO enrichment terms (Biological Process) of up-regulated DEGs from TCGA and CGGA database. B. In vitro VM formation assay (above panel) indicated the tube formation ability of cells overexpressing or silencing Prrx1. Transwell assay indicated the migration (middle panel) and invasion (below panel) ability of cells overexpressing or silencing Prrx1. C. RT-qPCR analyses revealed the transcriptional levels of SOX2 and CD31 during VM formation in LN229 and U251 cells.

CGGA693	Prrx1	SOX2	MMP2	VEGFA	TGFβ1	ABCC1
Prrx1	0.0000000	0.7038676	0.5098365	0.3360532	0.4715814	0.5519199
SOX2	0.7038676	0.0000000	0.3148933	0.3187757	0.2627119	0.4749706
MMP2	0.5098365	0.3148933	0.0000000	0.4494736	0.6124188	0.4486542
VEGFA	0.3360532	0.3187757	0.4494736	0.0000000	0.1515920	0.6396679
TGFβ1	0.4715814	0.2627119	0.6124188	0.1515920	0.0000000	0.2987663
ABCC1	0.5519199	0.4749706	0.4486542	0.6396679	0.2987663	0.0000000

GSE4290	Prrx1	SOX2	MMP2	VEGFA	TGFβ1	ABCC1
Prrx1	0.0000000	0.6132229	0.4665589	0.2966893	0.4260522	0.2716085
SOX2	0.6132229	0.0000000	0.2534587	0.1342312	0.2696539	0.1900781
MMP2	0.4665589	0.2534587	0.0000000	0.5230492	0.6990446	0.3476122
VEGFA	0.2966893	0.1342312	0.5230492	0.0000000	0.4958756	0.4464959
TGFβ1	0.4260522	0.2696539	0.6990446	0.4958756	0.0000000	0.4206098
ABCC1	0.2716085	0.1900781	0.3476122	0.4464959	0.4206098	0.0000000

GSE4412	Prrx1	SOX2	MMP2	VEGFA	TGFβ1	ABCC1
Prrx1	0.0000000	0.4321076	0.2285453	0.3360805	0.3633524	0.1197558
SOX2	0.4321077	0.0000000	0.1078109	0.2662482	0.0139839	-0.0756963
MMP2	0.2285453	0.1078108	0.0000000	0.2296551	0.0710836	0.1288170
VEGFA	0.3360805	0.2662482	0.2296551	0.0000000	0.2579840	0.1663459
TGFβ1	0.3633525	0.0139839	0.0710836	0.2579840	0.0000000	0.1991609
ABCC1	0.1197559	-0.0756963	0.1288170	0.1663459	0.1991609	0.0000000

GSE13041	Prrx1	SOX2	MMP2	VEGFA	TGFβ1	ABCC1
Prrx1	0.0000000	0.4179910	0.1682441	0.4208128	0.2997582	0.1569476
SOX2	0.4179911	0.0000000	0.0536448	0.2045366	0.0585017	0.1237990
MMP2	0.1682441	0.0536448	0.0000000	0.2179307	0.5034127	0.1661039
VEGFA	0.4208128	0.2045366	0.2179306	0.0000000	0.5637399	-0.3219173
TGFβ1	0.2997582	0.0585017	0.5034127	0.5637399	0.0000000	-0.0572970
ABCC1	0.1569476	0.1237990	0.1661039	-0.3219174	-0.0572970	0.0000000

GSE42669	Prrx1	SOX2	MMP2	VEGFA	TGFβ1	ABCC1
Prrx1	0.0000000	0.4313440	0.5880780	0.3839806	0.4565899	0.4949591
SOX2	0.4313440	0.0000000	0.3300124	0.3671100	-0.1474081	0.2949686
MMP2	0.5880780	0.3300124	0.0000000	0.3494529	0.3083508	0.4732231
VEGFA	0.3839806	0.3671100	0.3494529	0.0000000	0.2633443	0.4258409
TGFβ1	0.4565899	-0.1474081	0.3083508	0.2633443	0.0000000	0.4425842
ABCC1	0.4949591	0.2949686	0.4732231	0.4258409	0.4425842	0.0000000

TCGA	Prrx1	SOX2	MMP2	VEGFA	TGFβ1	ABCC1
Prrx1	0.0000000	0.31266895	0.33987033	0.3398653	0.5863460	0.5209744
SOX2	0.3126690	0.00000000	0.08241587	0.3201911	0.2855718	0.2698881
MMP2	0.3398703	0.08241587	0.00000000	0.2702059	0.4618489	0.2347458
VEGFA	0.3398653	0.32019109	0.27020585	0.0000000	0.3264932	0.3386773
TGFβ1	0.5863460	0.28557180	0.46184894	0.3264932	0.0000000	0.4970362
ABCC1	0.5209744	0.26988814	0.23474578	0.3386773	0.4970362	0.0000000

Supplementary Figure 2. Correlation coefficient matrix of gene expression levels.